

Fractional yields inferred from halo and thick disk stars

R. Caimmi*

May 12, 2019

Abstract

Linear $[Q/H]$ - $[O/H]$ relations, $Q = \text{Na, Mg, Si, Ca, Ti, Cr, Fe, Ni}$, are inferred from a sample ($N = 67$) of recently studied FGK-type dwarf stars in the solar neighbourhood including different populations (Nissen and Schuster 2010; Ramirez et al. 2012), namely LH ($N = 24$, low- α halo), HH ($N = 25$, high- α halo), KD ($N = 16$, thick disk), OL ($N = 2$, globular cluster outliers). Regression line slope and intercept estimators and related variance estimators are determined. With regard to the straight line, $[Q/H] = a_Q[O/H] + b_Q$, sample stars display along a “main sequence”, $[Q, O] = [a_Q, b_Q, \Delta b_Q]$, leaving aside the two OL stars which, in most cases (e.g., Na), lie outside. A unit slope, $a_Q = 1$, implies Q is a primary element synthesised via SNII progenitors in presence of universal stellar initial mass function (defined as simple primary element). To this respect, Mg, Si, Ti, show $\hat{a}_Q = 1$ within $\mp 2\hat{\sigma}_{\hat{a}_Q}$; Cr, Fe, Ni, within $\mp 3\hat{\sigma}_{\hat{a}_Q}$; Na, Ca, within $\mp r\hat{\sigma}_{\hat{a}_Q}$, $r > 3$. The empirical, differential element abundance distributions are inferred from LH, HH, KD, HA = HH + KD subsamples, where related regression lines represent their theoretical counterparts within the framework of simple MCBR (multistage closed box + reservoir) chemical evolution models. Hence the fractional yields, \hat{p}_Q/\hat{p}_O , are determined and (as an example) a comparison is shown with their theoretical counterparts inferred from SNII progenitor nucleosynthesis

**Physics and Astronomy Department, Padua Univ., Vicolo Osservatorio 3/2, I-35122 Padova, Italy* email: roberto.caimmi@unipd.it fax: 39-049-8278212

under the assumption of a power-law stellar initial mass function. The generalized fractional yields, $C_Q = Z_Q/Z_O^{a_Q}$, are determined regardless of the chemical evolution model. The ratio of outflow to star formation rate is compared for different populations, in the framework of simple MCBR models. The opposite situation of element abundance variation entirely due to cosmic scatter is also considered under reasonable assumptions. The related differential element abundance distribution fits to the data as well as its counterpart inferred in the opposite limit of instantaneous mixing in presence of chemical evolution, while the latter is preferred for HA subsample.

keywords - *Galaxy: evolution* - *Galaxy: formation* - *stars: evolution* - *stars: formation*.

1 Introduction

Leaving aside the first three minutes after the birth of the universe, elements heavier than He, or metals, are synthesised within stars and returned to the interstellar medium via supernova (SN) explosions, with the addition of envelope loss from planetary nebulae. There are two main types of SN. SNII progenitors are main-sequence stars, massive ($m \gtrsim 10m_\odot$) and short-lived ($0.001 \lesssim \tau/\text{Gyr} \lesssim 0.01$), producing a wide variety of nuclides among which are α elements (traditionally, Mg, Si, Ca, Ti, with the addition of O) and Fe (e.g., Woosley and Weaver 1995; Kobayashi et al. 2011). SNIa progenitors are white dwarfs belonging to a binary system, less massive ($m \lesssim 1.4m_\odot$), generally long-living ($\tau \gtrsim 1\text{Gyr}$), which mainly produce Fe (e.g., Kobayashi et al. 1998; Kobayashi and Nomoto 2009).

Element production within stars has been a major research focus for many years concerning e.g., abundance ratios as a function of the metallicity (Wheeler et al. 1989), nucleosynthesis in massive ($11 \leq m/m_\odot \leq 40$) stars with solar and subsolar metal abundance (Woosley and Weaver 1995), chemical evolution of the solar neighbourhood for elements up to zinc (Timmes et al. 1995), α element production and comparison with the data from different populations (MacWilliam 1997), stellar evolution including close binaries (Wallerstein et al. 1997), chemical evolution of Galactic and extra Galactic populations (Venn et al. 2004), evolution of the isotope ratios of elemental abundances (from C to Zn) in different Galactic populations (Kobayashi et al. 2011).

The fractional logarithmic number abundance or, in short, number abundance, $[Q/\text{Fe}]$, where Q denotes a generic nuclide and, in particular, an α element, has been the subject of several investigations (e.g., Edvardsson et

al. 1993; Nissen and Schuster 1997; Fulbright 2002; Stephens and Boesgaard 2002; Gratton et al. 2003) for establishing if the distribution of $[Q/Fe]$ in different populations is continuous or bimodal. Less attention, however, has been devoted to the connection between number abundances, $[Q/H]$, which are related to the chemical evolution of a single element, Q , instead of a pair, Q_1, Q_2 , for fixed hydrogen abundance (e.g., Caimmi 2013; Carretta 2013).

Dealing with $\{O[Q_1/H][Q_2/H]\}$ plane instead of $\{O[Q_1/H][Q_2/Q_1]\}$ could be due to two orders of reasons, namely (i) avoiding that uncertainties in Q_1 reflect on both axes and (ii) fully exploiting the different sites of nucleosynthesis for Q_1 . For instance, a simple $[Na/H]$ - $[Fe/H]$ linear relation is expected keeping in mind Na is mainly produced via hydrostatic C-burning within SNII progenitors, proportionally to the initial metallicity of the parent star (e.g., Woosley and Weaver 1995). On the other hand, additional production could take place via proton-capture on Ne in H-burning at high temperature, which could explain Na overabundance detected in some globular cluster stars. For further details and additional references, an interested reader is addressed to a recent attempt (Carretta 2013).

According to the standard definition, a nuclide is primary when the yield is independent of the initial composition of the parent star and secondary if otherwise (e.g., Pagel and Tautvaisiene 1995). Let simple primary elements be defined as synthesised via SNII progenitors in presence of universal stellar initial mass function. Accordingly, the yield ratio of two selected simple primary elements, or fractional yield, maintains constant in time, which implies $Z_Q/Z = (Z_Q)_\odot/Z_\odot$, $Z = \sum Z_Q$.

Within the framework of MCBR (multistage closed box + reservoir) models (Caimmi 2011a; 2012a) in the linear limit (hereafter quoted as simple MCBR models), which well hold for simple primary elements, the fractional yield may be expressed by a short formula and then inferred from the data related to early populations, such as the halo and the low-metallicity ($[Fe/H] < -0.6$) thick disk. Star formation therein spanned for less than about 1 Gyr, implying an interstellar medium mainly enriched by SNII progenitors. Number abundances of several elements, namely O, Na, Mg, Si, Ca, Ti, Cr, Fe, Ni, can be inferred from recently studied samples of solar neighbourhood FGK-type dwarf stars (Nissen and Schuster 2010, hereafter quoted as NS10; Ramirez et al. 2012, hereafter quoted as Ra12).

The current note is devoted to (i) analysis of the dependence of $[Q/H]$ on $[O/H]$, where $Q \neq O$ is any among the elements mentioned above. To this aim, a general classification is introduced and constraints on the chemical evolution of related populations are inferred; (ii) determination of empirical, differential element abundance distribution from different subsamples, together with related theoretical counterparts in the framework of simple

MCBR models; (iii) evaluation of fractional yields and related parameters in the framework of simple MCBR models, including an example of comparison with theoretical counterparts, inferred from SNII progenitor nucleosynthesis under the assumption of power-law stellar initial mass function; (iv) determination of theoretical, differential element abundance distribution in the opposite limit of inhomogeneous mixing due to cosmic scatter obeying a Gaussian distribution where the mean and the variance are evaluated from related subsamples.

Basic informations on the data (NS10; Ra12) are provided in Section 2. The inferred $[Q/H]$ - $[O/H]$ relations are shown and classified in Section 3. The results are discussed in Section 4. The conclusion is presented in Section 5. Further details are illustrated in the Appendix.

2 The data

The data are taken from a sample ($N = 67$) of solar neighbourhood FGK-type dwarf stars in the metallicity range, $-1.6 < [Fe/H] < -0.4$, for which $[O/H]$ has been determined via a non-LTE analysis of the 777 nm OI triplet lines (Ra12), while $[Fe/H]$ and $[Q/Fe]$, $Q = Na, Mg, Si, Ca, Ti, Cr, Ni$, are already known from an earlier attempt (NS10). Subsamples are extracted from the parent sample according to different populations, as LH (low- $[\alpha/Fe]$ halo stars), HH (high- $[\alpha/Fe]$ halo stars), KD (thick disk stars), OL (globular cluster outliers). The related population is LH ($N = 24$), HH ($N = 25$), KD ($N = 16$), OL ($N = 2$), respectively. KD stars exhibit low abundances, $[Fe/H] < -0.6$. OL stars are included for completeness and to get a first idea on the trend shown with respect to the empirical $[Q/H]$ - $[O/H]$ relation inferred for LH, HH, KD stars.

The fractional number abundances, $[O/H]$ and $[Fe/H]$, are taken from related parent papers (NS10; Ra12) while the remaining are inferred from the parent paper (NS10) according to the standard relation, $[Q/H] = [Q/Fe] + [Fe/H]$, which completes the set of needed data. For further details and exhaustive presentation, an interested reader is referred to the parent papers (NS10; Ra12).

For sake of simplicity, low/high- $[\alpha/Fe]$ halo stars shall be quoted in the following as low/high- α halo stars, where “low/high- α ” has to be intended with respect to fixed $[Fe/H]$ (e.g., NS10; Conroy 2012).

3 Results

Oxygen is the most abundant metal in the universe and is mainly synthesised within SNII progenitors. For this reason, oxygen abundance is chosen here as reference abundance. The empirical $[Q/H]$ - $[O/H]$ relations, $Q = \text{Na, Mg, Si, Ca}$; $Q = \text{Ti, Cr, Fe, Ni}$; are plotted in Figs. 1 and 2, respectively, for LH, HH, KD, OL, subsamples. Also shown are the narrowest “main sequences”, $[Q,O] = [1, b_Q, \Delta b_Q]$, limited by the straight lines of slope, $a_Q = 1$, and intercepts, $b_Q \mp \Delta b_Q/2$, within which the data lie leaving outside OL stars. For two selected elements, Q_1 and Q_2 , a general classification reads $[Q_1, Q_2] = [a_{Q_1}, b_{Q_1}, \Delta b_{Q_1}]$ (Caimmi 2013). Though OL stars are far from the main sequence only for Na, still a similar trend is shown for the remaining elements too.

The dispersion of the data around a straight line of fixed slope can be evaluated from the width of the main sequence measured on the vertical axis, as the difference between the intercepts of related bounding straight lines, Δb_Q . An inspection of Figs. 1-2 shows the largest dispersion is exhibited by Na, $\Delta b_{\text{Na}} = 0.7$ dex, followed by Cr and Fe, $\Delta b_{\text{Cr}} = \Delta b_{\text{Fe}} = 0.5$ dex, and the remaining elements, $\Delta b_{\text{Mg}} = \Delta b_{\text{Si}} = \Delta b_{\text{Ca}} = \Delta b_{\text{Ti}} = \Delta b_{\text{Ni}} = 0.4$ dex.

For each plot, the regression line has been determined for LH, HH, KD subsamples using the bisector method (e.g., Isobe et al. 1990; Caimmi 2011b, 2012b) and the results are listed in Table 1. The same has been done for the HA = HH + KD subsample ($N = 41$) for exploiting the possibility of an inner halo-thick disk chemical evolution. An inspection of Table 1 shows the following.

- (1) Regression line slope estimators, \hat{a}_Q , for different populations, are consistent within about $\mp 2\hat{\sigma}_{\hat{a}_Q}$, with the exception of Fe where they agree within $\mp \hat{\sigma}_{\hat{a}_Q}$.
- (2) For a fixed element, regression line slope estimators may be consistent with the unit slope within $\mp \hat{\sigma}_{\hat{a}_Q}$ for all populations (Si) or some (Ti) or only one (Na, Mg, Ca, Fe, Ni) or none (Cr). For all elements, regression line slope estimators may be consistent with the unit slope, regardless of the population, within $\mp 2\hat{\sigma}_{\hat{a}_Q}$ (Mg, Si, Ti) or $\mp 3\hat{\sigma}_{\hat{a}_Q}$ (Cr, Fe, Ni) or not at all i.e. $\mp r\hat{\sigma}_{\hat{a}_Q}$, $r > 3$ (Na, Ca).
- (3) Regression line intercept estimators, \hat{b}_Q , for different populations, may be consistent within $\mp \hat{\sigma}_{\hat{b}_Q}$ (Ti, Ni) or $\mp 2\hat{\sigma}_{\hat{b}_Q}$ (Na, Mg, Si, Ca) or marginally consistent within about $\mp 3\hat{\sigma}_{\hat{b}_Q}$ (Cr, Fe).

In conclusion, number abundances plotted in Figs. 1-2 show a linear trend

Table 1: Regression line slope estimator, \hat{a}_Q , square root of variance estimator, $\hat{\sigma}_{\hat{a}_Q}$, regression line intercept estimator, \hat{b}_Q , square root of variance estimator, $\hat{\sigma}_{\hat{b}_Q}$, generalized fractional yield, C_Q , expressed by Eq. (10), for $Q = \text{Na, Mg, Si, Ca, Ti, Cr, Fe, Ni}$, with regard to different subsamples, LH (low- α halo stars), HH (high- α halo stars), KD (low-metallicity thick disk stars), HA (high- α halo + low-metallicity thick disk stars). See text for further details.

| Q | \hat{a}_Q | $\hat{\sigma}_{\hat{a}_Q}$ | $-\hat{b}_Q$ | $\hat{\sigma}_{\hat{b}_Q}$ | C_Q | pop |
|----|-------------|----------------------------|--------------|----------------------------|------------|-----|
| Na | 1.1467D+00 | 1.1017D-01 | 4.9224D-01 | 9.6151D-02 | 3.4952D-03 | LH |
| | 1.3461D+00 | 5.1060D-02 | 3.3485D-01 | 2.9875D-02 | 1.4034D-02 | HH |
| | 1.3036D+00 | 1.4981D-01 | 3.1286D-01 | 5.4564D-02 | 1.1857D-02 | KD |
| | 1.3339D+00 | 5.4134D-02 | 3.2406D-01 | 2.5128D-02 | 1.3508D-02 | HA |
| Mg | 9.3798D-01 | 4.8701D-02 | 2.6995D-01 | 4.1267D-02 | 4.8194D-02 | LH |
| | 1.0333D+00 | 3.4714D-02 | 1.6663D-01 | 1.9884D-02 | 9.9892D-02 | HH |
| | 1.0916D+00 | 5.2829D-02 | 1.4288D-01 | 2.3186D-02 | 1.4250D-01 | KD |
| | 1.0464D+00 | 3.0344D-02 | 1.6189D-01 | 1.5833D-02 | 1.0805D-01 | HA |
| Si | 9.1887D-01 | 4.1941D-02 | 2.8057D-01 | 3.5713D-02 | 4.0039D-02 | LH |
| | 9.7167D-01 | 4.4229D-02 | 2.2499D-01 | 2.1505D-02 | 5.9734D-02 | HH |
| | 1.0258D+00 | 4.1416D-02 | 2.0678D-01 | 2.1943D-02 | 8.2335D-02 | KD |
| | 9.8441D-01 | 3.5638D-02 | 2.2186D-01 | 1.7139D-02 | 6.4237D-02 | HA |
| Ca | 9.3394D-01 | 4.5183D-02 | 1.7341D-01 | 3.5430D-02 | 5.3438D-03 | LH |
| | 9.3210D-01 | 3.2634D-02 | 2.3770D-01 | 1.7615D-02 | 4.5650D-03 | HH |
| | 1.0244D+00 | 4.4200D-02 | 2.3114D-01 | 1.9383D-02 | 7.4573D-03 | KD |
| | 9.5927D-01 | 3.2646D-02 | 2.3965D-01 | 1.4921D-02 | 5.2271D-03 | HA |
| Ti | 8.7152D-01 | 5.2099D-02 | 3.0866D-01 | 3.7487D-02 | 1.3807D-04 | LH |
| | 1.0007D+00 | 3.5937D-02 | 2.6133D-01 | 1.7091D-02 | 2.9955D-04 | HH |
| | 1.0667D+00 | 7.5124D-02 | 2.5133D-01 | 2.8450D-02 | 4.3066D-04 | KD |
| | 1.0184D+00 | 3.3349D-02 | 2.6137D-01 | 1.4353D-02 | 3.2808D-04 | HA |
| Cr | 1.1622D+00 | 4.5627D-02 | 2.8681D-01 | 3.3824D-02 | 3.4549D-03 | LH |
| | 1.1459D+00 | 3.5077D-02 | 4.4373D-01 | 1.8743D-02 | 2.2135D-03 | HH |
| | 1.1823D+00 | 7.0671D-02 | 4.4678D-01 | 3.2115D-02 | 2.6505D-03 | KD |
| | 1.1569D+00 | 3.2707D-02 | 4.4658D-01 | 1.6126D-02 | 2.3264D-03 | HA |
| Fe | 1.1311D+00 | 4.2032D-02 | 2.9019D-01 | 3.6276D-02 | 2.2724D-01 | LH |
| | 1.0849D+00 | 3.9103D-02 | 4.8509D-01 | 2.3072D-02 | 1.1430D-01 | HH |
| | 1.1035D+00 | 6.7964D-02 | 4.7888D-01 | 3.1622D-02 | 1.2766D-01 | KD |
| | 1.0892D+00 | 3.4539D-02 | 4.8406D-01 | 1.8746D-02 | 1.1715D-01 | HA |
| Ni | 1.0165D+00 | 5.3955D-02 | 4.7925D-01 | 4.3627D-02 | 4.4933D-03 | LH |
| | 1.1406D+00 | 3.7857D-02 | 4.6429D-01 | 2.3555D-02 | 8.8122D-03 | HH |
| | 1.1400D+00 | 7.4321D-02 | 4.5788D-01 | 3.2996D-02 | 8.9152D-03 | KD |
| | 1.1396D+00 | 3.4006D-02 | 4.6208D-01 | 1.8954D-02 | 8.8146D-03 | HA |

as:

$$[Q/H] = a_Q [O/H] + b_Q ; \quad (1)$$

for LH, HH, KD, HA populations, according to Table 1. While different populations may be connected with the same regression line to a first extent, the consistency with the unit slope appears problematic in several cases.

By definition, $[O/Q] = [O/H] - [Q/H]$, which via Eq. (1) translates into:

$$[O/Q] = (1 - a_Q) [O/H] - b_Q ; \quad (2)$$

where, in particular, low- $[O/Q]$ stars relate to larger a_Q and/or b_Q with respect to high- $[O/Q]$ stars and, in addition, a constant $[O/Q]$ abundance ratio relates to the unit slope, $a_Q = 1$. According to the standard notation, $[Q_1/Q_2] = \log(N_{Q_1}/N_{Q_2}) - \log(N_{Q_1}/N_{Q_2})_\odot$, where N_Q is the number density of the element, Q.

The empirical differential abundance distribution, $\psi = \Delta N / (N \Delta \phi)$, inferred from HH, LH, KD, HA subsamples, is plotted in Figs. 3-11 for Q = O, Na, Mg, Si, Ca, Ti, Cr, Fe, Ni, respectively. Data are equally binned in $[Q/H]$ taking $\Delta[Q/H] = 1$ dex. Uncertainties in ψ , $\Delta^\mp \psi$, are calculated as Poissonian errors, which implies $\Delta^- \psi \rightarrow \infty$ for bins populated by a single star, $\Delta N = 1$. For further details, an interested reader is addressed to earlier attempts (e.g., Caimmi 2011a, 2012a).

The theoretical differential abundance distribution, predicted by simple MCBR models, is a straight line (e.g., Caimmi 2011a, 2012a) expressed as:

$$\psi = \frac{dN}{N d\phi} = \alpha_Q \phi + \beta_Q ; \quad (3)$$

with regard to a selected element, Q.

Keeping in mind errors in ψ are dominating on errors in ϕ , as shown in Figs. 3-11, regression lines have been determined using standard least square methods (e.g., Isobe et al. 1990; Caimmi 2011b, 2012b), leaving aside points related to bins populated by a single star, where $\Delta^- \psi \rightarrow \infty$. The regression procedure has been performed on LH, HH, KD, HA subsamples and the results are shown in Table 2. The main features are listed below.

- (1) Regression line slope estimators, $\hat{\alpha}_Q$, are systematically lower for HH population with respect to LH and KD population even if, in some cases, they agree within $\mp \hat{\sigma}_{\hat{\alpha}_Q}$.
- (2) For a fixed element, regression line slope estimators may be consistent within $\mp \hat{\sigma}_{\hat{\alpha}_Q}$ for two populations at most, among LH, HH, KD.

Table 2: Regression line slope estimator, $\hat{\alpha}_Q$, square root of variance estimator, $\hat{\sigma}_{\hat{\alpha}_Q}$, regression line intercept estimator, $\hat{\beta}_Q$, square root of variance estimator, $\hat{\sigma}_{\hat{\beta}_Q}$, for $Q = \text{O, Na, Mg, Si, Ca, Ti, Cr, Fe, Ni}$, with regard to different subsamples, LH (low- α halo stars), HH (high- α halo stars), KD (low-metallicity thick disk stars), HA (high- α halo + low-metallicity thick disk stars). Bins populated by a single star were not considered in performing the regression procedure. See text for further details.

| Q | $\hat{\alpha}_Q$ | $\hat{\sigma}_{\hat{\alpha}_Q}$ | $\hat{\beta}_Q$ | $\hat{\sigma}_{\hat{\beta}_Q}$ | pop |
|----|------------------|---------------------------------|-----------------|--------------------------------|-----|
| O | 1.2395825D-00 | 4.0782960D-01 | 7.6627742D-01 | 8.4978932D-02 | LH |
| | 4.7980024D-01 | 1.6648632D-01 | 4.0664611D-01 | 8.6555380D-02 | HH |
| | 1.5989830D-00 | 1.6397793D-01 | 9.1710570D-01 | 6.9667135D-02 | KD |
| | 4.7090995D-01 | 1.8054961D-01 | 3.1723663D-01 | 8.8226620D-02 | HA |
| Na | 7.7450493D-00 | 2.5744210D-00 | 1.6707642D-00 | 1.4708321D-01 | LH |
| | 2.1093278D-00 | 7.3885505D-01 | 9.9040108D-01 | 1.4996766D-01 | HH |
| | 2.9245562D-00 | 5.2163677D-01 | 1.2998827D-00 | 9.4153768D-02 | KD |
| | 1.9183122D-00 | 5.1304826D-01 | 8.7072663D-01 | 9.6271620D-02 | HA |
| Mg | 4.0671532D-00 | 1.0343054D-00 | 1.3231002D-00 | 1.3072240D-01 | LH |
| | 1.1714832D-00 | 2.8303357D-01 | 6.5642583D-01 | 1.0927166D-01 | HH |
| | 2.3635566D-00 | 3.5784751D-01 | 1.1661197D-00 | 1.1649145D-01 | KD |
| | 1.1487217D-00 | 4.2325854D-01 | 6.3913599D-01 | 1.4635049D-01 | HA |
| Si | 3.8998171D-00 | 8.1562678D-01 | 1.2767069D-00 | 1.0525175D-01 | LH |
| | 7.7173538D-01 | 3.2248529D-01 | 5.3136082D-01 | 1.0414279D-01 | HH |
| | 1.5024742D-00 | 4.5603650D-01 | 8.4982713D-01 | 1.2099418D-01 | KD |
| | 7.7174327D-01 | 3.2248262D-01 | 3.1651458D-01 | 1.0414213D-01 | HA |
| Ca | 1.8159479D-00 | 5.1939008D-01 | 1.0003550D-00 | 8.4484996D-02 | LH |
| | 7.3263802D-01 | 3.6421500D-01 | 5.2426101D-01 | 1.2156292D-01 | HH |
| | 1.9471117D-00 | 8.5169618D-01 | 1.1180379D-01 | 2.1662050D-01 | KD |
| | 1.9437007D-00 | 9.4067715D-01 | 7.6334270D-01 | 2.1532687D-01 | HA |
| Ti | 2.6360692D-00 | 1.1883298D-00 | 1.0953549D-00 | 1.5262722D-01 | LH |
| | 1.3332657D-00 | 3.7333476D-01 | 7.0231670D-01 | 1.1503626D-01 | HH |
| | 3.0193634D-00 | 8.9886183D-01 | 1.4421308D-00 | 2.3278547D-01 | KD |
| | 1.8605943D-00 | 6.6369903D-01 | 8.5576686D-01 | 1.8685473D-01 | HA |
| Cr | 5.4302264D-00 | 8.2726991D-01 | 1.3218599D-00 | 7.5469008D-02 | LH |
| | 2.7808727D-00 | 6.9731467D-01 | 1.0312708D-00 | 1.3312629D-01 | HH |
| | 4.5413461D-00 | 1.3250681D-00 | 1.4005244D-00 | 1.7536734D-01 | KD |
| | 3.9361698D-00 | 8.3118178D-01 | 1.0738609D-00 | 1.3953063D-01 | HA |
| Fe | 3.9164513D-00 | 1.2277461D-00 | 1.2025410D-00 | 1.1751637D-01 | LH |
| | 2.4722723D-00 | 7.3136235D-01 | 1.0575561D-00 | 1.2057248D-01 | HH |
| | 3.0259847D-00 | 1.4404427D-00 | 1.2143858D-00 | 2.0069136D-01 | KD |
| | 2.1992895D-00 | 1.0676311D-00 | 9.3872327D-01 | 1.5758267D-01 | HA |
| Ni | 7.3799819D-00 | 1.3454868D-00 | 1.5095290D-00 | 1.0090129D-01 | LH |
| | 2.6592341D-00 | 9.6597500D-01 | 1.1044067D-00 | 1.6598601D-01 | HH |
| | 4.2832478D-00 | 6.2974963D-01 | 1.3132038D-00 | 9.6973684D-02 | KD |
| | 2.6455002D-00 | 8.3327832D-01 | 1.0344389D-00 | 1.3131387D-01 | HA |

- (3) Regression line intercept estimators, $\hat{\beta}_Q$, are systematically lower for HH population with respect to both LH and KD population even if, in some cases, they agree within $\mp \hat{\sigma}_{\hat{\beta}_Q}$.

In conclusion, empirical differential abundance distributions plotted in Figs. 3-11 show a linear trend, as expressed by Eq. (3), leaving aside bins populated by a single star.

Arithmetic mean and rms error can be inferred from the above mentioned distributions as:

$$\overline{\log \phi_Q} = \overline{[Q/H]} = \frac{1}{N} \sum_{i=1}^N [Q/H]_i ; \quad (4)$$

$$\sigma_{\log \phi_Q} = \sigma_{[Q/H]} = \left\{ \frac{1}{N-1} \sum_{i=1}^N ([Q/H]_i - \overline{[Q/H]})^2 \right\}^{1/2} ; \quad (5)$$

where N is the sample population. Related values for each element, Q, and subsample, LH, HH, KD, HA, are listed in Table 3.

4 Discussion

While number abundances, $[Q_1/Q_2]$, can be inferred from observations, predictions from chemical evolution models concern mass abundances, $Z_Q = m_Q/m$, where m_Q is the total mass in the element, Q, and $m = \sum m_Q$ is the total mass.

The normalized mass abundance, ϕ_Q , and the number abundance, $[Q/H]$, may be related as (e.g., Caimmi 2007):

$$\log \frac{\phi_Q}{\phi_H} = [Q/H] ; \quad (6)$$

$$\phi_Q = \frac{Z_Q}{(Z_Q)_\odot} ; \quad \phi_H = \frac{X}{X_\odot} ; \quad (7)$$

where $X = Z_H$ according to the standard notation.

The substitution of Eq. (6) into the linear fit to the data, Eq. (1), yields after some algebra:

$$\frac{\phi_Q}{\phi_H} = \exp_{10}(b_Q) \left(\frac{\phi_Q}{\phi_H} \right)^{a_Q} ; \quad (8)$$

which, in terms of mass abundances, via Eq. (7) translates into:

$$Z_Q = C_Q (Z_O)^{a_Q} ; \quad (9)$$

$$C_Q = \exp_{10}(b_Q) \frac{(Z_Q)_\odot}{[(Z_O)_\odot]^{a_Q}} \left(\frac{X}{X_\odot} \right)^{1-a_Q} ; \quad (10)$$

Table 3: Star number, N , mean abundance, $\overline{[Q/H]}$, rms error, $\sigma_{[Q/H]}$, $Q = O, Na, Mg, Si, Ca, Ti, Cr, Fe, Ni$, inferred for different subsamples, LH (low- α halo stars), HH (high- α halo stars), KD (low-metallicity thick disk stars), HA (high- α halo + low-metallicity thick disk stars). See text for further details.

| Q | N | $\overline{[Q/H]}$ | $\sigma_{[Q/H]}$ | pop |
|----|-----|--------------------|------------------|-----|
| O | 24 | -0.7517 | 0.2260 | LH |
| | 25 | -0.4020 | 0.3011 | HH |
| | 16 | -0.4394 | 0.2007 | KD |
| | 41 | -0.4166 | 0.2643 | HA |
| Na | 24 | -1.3542 | 0.2595 | LH |
| | 25 | -0.8760 | 0.4054 | HH |
| | 16 | -1.4981 | 3.1286 | KD |
| | 41 | -0.8798 | 0.3526 | HA |
| Mg | 24 | -0.9750 | 0.2120 | LH |
| | 25 | -0.5820 | 0.3111 | HH |
| | 16 | -0.6225 | 0.2191 | KD |
| | 41 | -0.5978 | 0.2766 | HA |
| Si | 24 | -0.9713 | 0.2077 | LH |
| | 25 | -0.6156 | 0.2926 | HH |
| | 16 | -0.6575 | 0.2059 | KD |
| | 41 | -0.6320 | 0.2602 | HA |
| Ca | 24 | -0.8754 | 0.2111 | LH |
| | 25 | -0.6124 | 0.2807 | HH |
| | 16 | -0.6813 | 0.2056 | KD |
| | 41 | -0.6393 | 0.2535 | HA |
| Ti | 24 | -0.9638 | 0.1969 | LH |
| | 25 | -0.6636 | 0.3013 | HH |
| | 16 | -0.7200 | 0.2141 | KD |
| | 41 | -0.6856 | 0.2692 | HA |
| Cr | 24 | -1.1604 | 0.2627 | LH |
| | 25 | -0.9044 | 0.3451 | HH |
| | 16 | -0.9663 | 0.2373 | KD |
| | 41 | -0.9285 | 0.3058 | HA |
| Fe | 24 | -1.1404 | 0.2557 | LH |
| | 25 | -0.9228 | 0.3264 | HH |
| | 16 | -0.9638 | 0.2215 | KD |
| | 41 | -0.9388 | 0.2877 | HA |
| Ni | 24 | -1.2433 | 0.2298 | LH |
| | 25 | -0.9228 | 0.3435 | HH |
| | 16 | -0.9588 | 0.2288 | KD |
| | 41 | -0.9368 | 0.3012 | HA |

where the dependence on X may be neglected for a_Q sufficiently close to unity and/or X sufficiently close to X_\odot . Accordingly, the coefficient, $C_Q = Z_Q/(Z_O)^{a_Q}$, may be conceived as a fractional generalized yield. Related values, inferred from the data using recent determinations of solar abundances and isotopic fractions (Asplund et al. 2009), are listed in Table 1. A formal calculation of solar photospheric mass abundances is shown in Appendix A.

The special case, $a_Q = 1$, implies a linear relation between Z_Q and Z_O . Accordingly, Q and O are simple primary elements. Conversely, a_Q different from unity outside (arbitrarily chosen) $\mp 2\sigma_{a_Q}$ implies non-simple primary elements (i.e. appreciably synthesised outside SNII progenitors or in absence of universal stellar initial mass function) or secondary elements.

With regard to simple chemical evolution models, the assumption of instantaneous recycling and universal stellar initial mass function implies fiducial predictions for simple primary elements. The special case of simple MCBR models reads (Caimmi 2011a):

$$\phi_Q - (\phi_Q)_i = -\frac{\hat{p}_Q}{(1+\kappa)(Z_Q)_\odot} \ln \frac{\mu}{\mu_i} ; \quad (11)$$

$$\phi_O - (\phi_O)_i = -\frac{\hat{p}_O}{(1+\kappa)(Z_O)_\odot} \ln \frac{\mu}{\mu_i} ; \quad (12)$$

where κ is the flow parameter, positive for outflow and negative for inflow, μ is the fractional active (i.e. viable for star formation) gas mass normalized to the initial mass, and the index, i , denotes values at the starting configuration. Accordingly, the fractional yield, \hat{p}_Q/\hat{p}_O , can be expressed as:

$$\frac{\hat{p}_Q}{\hat{p}_O} = \frac{Z_Q[1 - (Z_Q)_i/Z_Q]}{Z_O[1 - (Z_O)_i/Z_O]} = \frac{Z_Q}{Z_O} ; \quad (13)$$

which is owing to a further assumption of MCBR models, that all elements are simple primary i.e. constant ratio, Z_Q/Z , $Z = \sum Z_Q$ (Caimmi 2011a) implying, in turn, constant ratio, Z_Q/Z_O . A formal calculation is shown in Appendix B.

The substitution of Eq. (13) into (8), the last particularized to the unit slope, produces:

$$\frac{\hat{p}_Q}{\hat{p}_O} = \frac{(Z_Q)_\odot}{(Z_O)_\odot} \exp_{10}(b_Q) ; \quad (14)$$

where the intercepts, b_Q , are listed in Table 1. In conclusion, simple MCBR chemical evolution models imply $a_Q = 1$.

Let a generic element, $Q \neq O$, be considered as simple primary if the regression line slope estimator, inferred from the empirical $[Q/H]$ - $[O/H]$ relation, is consistent with the unit slope within $\mp 2\hat{\sigma}_{a_Q}$. With regard to the

subsamples studied in the current attempt, an inspection of Table 1 shows the following elements are inferred from the data to be simple primary. LH: Ni within $\mp 1\hat{\sigma}_{\hat{a}_Q}$ and Na, Mg, Si, Ca, Ti, within $\mp 2\hat{\sigma}_{\hat{a}_Q}$, while Cr and Fe are excluded. HH: Mg, Si, Ti, within $\mp 1\hat{\sigma}_{\hat{a}_Q}$ and Ca within about $\mp 2\hat{\sigma}_{\hat{a}_Q}$, while Na, Cr, Fe, Ni, are excluded. KD: Si, Ca, Ti, within $\mp 1\hat{\sigma}_{\hat{a}_Q}$ and Mg, Fe, Ni, within $\mp 2\hat{\sigma}_{\hat{a}_Q}$, while Na and Cr are excluded. Then α elements (Mg, Si, Ca, Ti) together with Na, Ni, for LH stars and Fe, Ni, for KD stars, are inferred from the data to be simple primary elements, which does not hold for Na (HH and KD stars), Cr (LH, HH and KD stars), Fe (LH and HH stars), Ni (HH stars).

Keeping in mind $Z_Q \ll 1$, an exponent, $a_Q > 1$, appearing in Eq. (9), implies Z_Q grows at an increasing rate with respect to Z_O , as expected for non-simple primary or secondary elements. In this view, Na, Cr, Fe, Ni, could be conceived as non-simple primary or secondary elements, which implies $[O/Q]$ is decreasing in time, as shown by the data (e.g., Ra12, Fig. 8 therein).

An empirical $[Na/H]$ - $[Fe/H]$ relation has been inferred from a large ($N = 1891$) sample in a recent attempt (Carretta 2013). Aiming to a comparison with the current results, the particularization of Eq. (1) to $Q = Na, Fe$, after elimination of $[O/H]$ yields:

$$[Na/H] = A[Fe/H] + B \quad ; \quad (15)$$

$$A = \frac{a_{Na}}{a_{Fe}} \quad ; \quad B = b_{Na} - Ab_{Fe} \quad ; \quad (16)$$

where the values of the coefficients on the right-hand side are listed in Table 1 for different subsamples. Accordingly, A and B can be evaluated for the “main sequences” on the $\{O[O/H][Na/H]\}$ and $\{O[O/H][Fe/H]\}$ plane described in a recent attempt (Caimmi 2013)¹. Starting from $a_{Fe} = 1$, $b_{Fe} = -0.45, -0.70, -0.20$; $a_{Na} = 1.25$, $b_{Na} = -0.40, -0.70, -0.10$; (Caimmi 2013), the result is $A = 1.25$, $B = 0.1625, -0.4000, 0.7250$. For subsamples considered in the current paper, A and B can be directly evaluated by determining the regression line on the $\{O[Fe/H][Na/H]\}$ plane. The results are listed in Table 4.

Related $[Na/H]$ - $[Fe/H]$ relations can be plotted as straight lines and compared with their counterparts inferred from the large sample (Carretta 2013). Unfortunately, the regression line is not expressed therein and the comparison has to be made by eye. Interestingly, outliers specified within the large sample (Carretta 2013) could be related to LH population. An inspection of Table 4 shows a lower slope for LH subsample with respect to the other ones

¹The main sequence in the caption of Fig. 2 therein is expressed as $[Na/H] = [Fe/H] - 0.4 \pm 0.3$ instead of $[Na/H] = 1.25[Fe/H] - 0.4 \pm 0.3$, due to a printing error.

Table 4: Regression line slope estimator, \hat{A} , square root of variance estimator, $\hat{\sigma}_{\hat{A}}$, regression line intercept estimator, \hat{B} , square root of variance estimator, $\hat{\sigma}_{\hat{B}}$, inferred from the data with regard to different subsamples, LH (low- α halo stars), HH (high- α halo stars), KD (low-metallicity thick disk stars), HA (high- α halo + low-metallicity thick disk stars), and the total sample with the exclusion of OL stars, HK = LH+HH+KD. See text for further details.

| \hat{A} | $\hat{\sigma}_{\hat{A}}$ | \hat{B} | $\hat{\sigma}_{\hat{B}}$ | pop |
|---------------|--------------------------|----------------|--------------------------|-----|
| 1.0147770D-00 | 8.2903367D-02 | -1.9689805D-01 | 1.0642713D-01 | LH |
| 1.2409084D-00 | 3.5227278D-02 | +2.6712483D-01 | 3.1356340D-02 | HH |
| 1.1821507D-00 | 7.6558086D-02 | +2.5367275D-01 | 6.2117800D-02 | KD |
| 1.2248702D-00 | 3.7797350D-02 | +2.6893320D-01 | 3.2037882D-02 | HA |
| 1.3043300D-00 | 5.5544051D-02 | +2.1084026D-01 | 6.4229880D-02 | HK |

and, in fact, outliers exhibit lower slope with respect to “normal” stars (Carretta 2013, Fig. 5 therein, bottom panel). In addition, it can be seen most stars belonging to the large sample lie within the main sequence, $[\text{Na}/\text{H}] = 1.25 [\text{Fe}/\text{H}] + 0.1625 \pm 0.5625$, with the exception of a few Na-overabundant, low-metallicity stars which, to this respect, should be considered as “outliers” instead of Na-deficient, low-metallicity stars.

Turning to the whole set of elements considered in the current attempt, it would be relevant investigating to what extent simple MCBR models fit to the data. With regard to a selected element, Q, the slope of the theoretical differential abundance distribution, expressed by Eq. (3), can be explicitly written as (e.g., Caimmi 2011a, 2012a):

$$\alpha_Q = -\frac{1 + \kappa(Z_Q)_\odot}{\ln 10} \frac{(Z_Q)_\odot}{\hat{p}_Q} ; \quad (17)$$

and the ratio of the terms on both sides of Eq. (17) to their counterparts particularized to oxygen, Q = O, after little algebra yields:

$$\frac{\hat{p}_Q}{\hat{p}_O} = \frac{(Z_Q)_\odot}{(Z_O)_\odot} \frac{\alpha_O}{\alpha_Q} ; \quad (18)$$

to be compared with Eq. (14). Related rms errors are expressed in Appendix C, Eqs. (36) and (34), respectively. The results are shown in Table 5 for Q = Na, Mg, Si, Ca, Ti, Cr, Fe, Ni, with regard to LH, HH, KD, HA subsamples. An inspection of Table 5 discloses the following.

Table 5: Fractional yield, \hat{p}_Q/\hat{p}_O , inferred from the data in the light of simple MCBR models via Eqs. (14), (18), related rms error, $\hat{\sigma}_{\hat{p}_Q/\hat{p}_O}$, inferred from Eqs. (34), (36), respectively, intercept of the straight line, b_Q , expressed by Eq. (1), inferred from the data in the light of simple MCBR models via Eq. (19), related rms error inferred from Eq. (38), for Q = Na, Mg, Si, Ca, Ti, Cr, Fe, Ni, with regard to different subsamples, LH (low- α halo stars), HH (high- α halo stars), KD (low-metallicity thick disk stars), HA (high- α halo + low-metallicity thick disk stars). See text for further details.

| Q | \hat{p}_Q/\hat{p}_O | $\sigma_{\hat{p}_Q/\hat{p}_O}$ | \hat{p}_Q/\hat{p}_O | $\sigma_{\hat{p}_Q/\hat{p}_O}$ | $-b_Q$ | σ_{b_Q} |
|----|-----------------------|--------------------------------|-----------------------|--------------------------------|-------------|----------------|
| Na | 1.6415D-03 | 1.3709D-04 | 8.1601D-04 | 3.8164D-04 | +7.9575D-01 | 2.0311D-01 |
| | 2.3585D-03 | 6.1201D-05 | 1.1597D-03 | 3.7181D-04 | +6.4308D-01 | 2.1413D-01 |
| | 2.4810D-03 | 1.1758D-04 | 2.7876D-03 | 5.7353D-04 | +2.6222D-01 | 8.9354D-02 |
| | 2.4176D-03 | 5.2766D-05 | 1.2516D-03 | 5.8508D-04 | +6.0998D-01 | 2.0302D-01 |
| Mg | 6.6340D-02 | 2.3779D-03 | 3.7642D-02 | 1.5653D-02 | +5.1602D-01 | 1.8059D-01 |
| | 8.4159D-02 | 1.4535D-03 | 5.0584D-02 | 2.1388D-02 | +3.8768D-01 | 1.8363D-01 |
| | 8.8889D-02 | 1.7901D-03 | 8.3553D-02 | 1.5279D-02 | +1.6972D-01 | 7.9417D-02 |
| | 8.5074D-02 | 1.1700D-03 | 5.0630D-02 | 2.6923D-02 | +3.8728D-01 | 2.3094D-01 |
| Si | 6.0818D-02 | 1.9922D-03 | 3.6878D-02 | 1.4377D-02 | +4.9777D-01 | 1.6931D-01 |
| | 6.9121D-02 | 1.2911D-03 | 7.2132D-02 | 3.9179D-02 | +2.0641D-01 | 2.3589D-01 |
| | 7.2081D-02 | 1.3738D-03 | 1.2347D-01 | 3.9559D-02 | -2.7037D-02 | 1.3914D-01 |
| | 6.9611D-02 | 1.0363D-03 | 7.0795D-02 | 4.0148D-02 | +2.1453D-01 | 2.4629D-01 |
| Ca | 7.5105D-03 | 2.3113D-04 | 7.6425D-03 | 3.3317D-03 | +1.6583D-01 | 1.8933D-01 |
| | 6.4771D-03 | 9.9101D-05 | 7.3322D-03 | 4.4451D-03 | +1.8383D-01 | 2.6329D-01 |
| | 6.5755D-03 | 1.1070D-04 | 9.1942D-03 | 4.1307D-03 | +8.5547D-02 | 1.9512D-01 |
| | 6.4478D-03 | 8.3565D-05 | 2.7125D-03 | 1.6748D-03 | +6.1569D-01 | 2.6815D-01 |
| Ti | 2.6767D-04 | 8.7155D-06 | 2.5617D-04 | 1.4296D-04 | +3.2768D-01 | 2.4237D-01 |
| | 2.9850D-04 | 4.4312D-06 | 1.9604D-04 | 8.7412D-05 | +4.4386D-01 | 1.9364D-01 |
| | 3.0545D-04 | 7.5481D-06 | 2.8849D-04 | 9.0837D-05 | +2.7607D-01 | 1.3675D-01 |
| | 2.9843D-04 | 3.7205D-06 | 1.3788D-04 | 7.2204D-05 | +5.9671D-01 | 2.2743D-01 |
| Cr | 1.4977D-03 | 4.4001D-05 | 6.6163D-04 | 2.3988D-04 | +6.4154D-01 | 1.5746D-01 |
| | 1.0435D-03 | 1.6988D-05 | 5.0007D-04 | 2.1409D-04 | +7.6312D-01 | 1.8593D-01 |
| | 1.0362D-03 | 2.8905D-05 | 1.0205D-03 | 3.1562D-04 | +4.5334D-01 | 1.3432D-01 |
| | 1.0365D-03 | 1.4518D-05 | 3.4675D-04 | 1.5178D-04 | +9.2214D-01 | 1.9010D-01 |
| Fe | 1.1563D-01 | 3.6434D-03 | 7.1386D-02 | 3.2441D-02 | +4.9962D-01 | 1.9736D-01 |
| | 7.3818D-02 | 1.4793D-03 | 4.3772D-02 | 1.9959D-02 | +7.1204D-01 | 1.9803D-01 |
| | 7.4881D-02 | 2.0567D-03 | 1.1918D-01 | 5.8035D-02 | +2.7702D-01 | 2.1148D-01 |
| | 7.3989D-02 | 1.2047D-03 | 4.8293D-02 | 2.9874D-02 | +6.6934D-01 | 2.6865D-01 |
| Ni | 4.1266D-03 | 1.5637D-04 | 2.0896D-03 | 7.8597D-04 | +7.7478D-01 | 1.6336D-01 |
| | 4.2712D-03 | 8.7387D-05 | 2.2446D-03 | 1.1276D-03 | +7.4370D-01 | 2.1817D-01 |
| | 4.3347D-03 | 1.2423D-04 | 4.6441D-03 | 8.3250D-04 | +4.2793D-01 | 7.7851D-02 |
| | 4.2930D-03 | 7.0677D-05 | 2.2144D-03 | 1.0988D-03 | +7.4957D-01 | 2.1550D-01 |

- (1) For assigned element, Q, and population, the results for \hat{p}_Q/\hat{p}_O are consistent within $\mp\sigma_{\hat{p}_Q/\hat{p}_O}$ or less, leaving aside Ca, Ti, Cr (LH, HH, HA), Ni (LH).
- (2) For assigned element, Q, the results for \hat{p}_Q/\hat{p}_O are consistent within $\mp2\sigma_{\hat{p}_Q/\hat{p}_O}$ or less for HH, KD, HA populations, while the contrary holds for LH population, which exhibits lower values with regard to Na, Mg, Si, Ti, higher values with respect to Ca, Cr, Fe, and nearly equal values for Ni, in connection with Eqs. (14) and (34).
- (3) A similar trend, partially hidden by larger errors, is shown via Eqs. (18) and (36). In particular, larger \hat{p}_{Fe}/\hat{p}_O values imply a lower [O/Fe] abundance ratio for LH population with respect to HH, KD, HA, as inferred from the data. Accordingly, MCBR models might provide a viable description of the chemical evolution of the halo and the (low-metallicity) thick disk.

A comparison between the fractional yield, \hat{p}_Q/\hat{p}_O , inferred from the data in the framework of simple MCBR models, and theoretical counterparts deduced from an earlier attempt (Woosley and Weaver 1995) is shown in Figs. 12 and 13 for $Q = \text{Na, Mg, Si, Ca}$, and $Q = \text{Ti, Cr, Fe, Ni}$, respectively, with regard to different subsamples (LH, HH, KD, HA) and different power-law stellar initial mass function exponents.

More specifically, horizontal bars represent fractional yields inferred from Eqs. (14) and (18), top and bottom, respectively, where the semiamplitude equals $2\sigma_{\hat{p}_Q/\hat{p}_O}$ in each case, as listed in Table 5. Full and dashed vertical bands represent theoretical fractional yields deduced from SNII progenitor nucleosynthesis within the mass range, $11 \leq m/m_\odot \leq 40$, $Z = Z_\odot$, and $12 \leq m/m_\odot \leq 40$, $Z = Z_\odot/10$, respectively (Woosley and Weaver 1995, model A), where the power-law stellar initial mass function exponent, p , lies within the range, $-3 \leq -p \leq -2$. A narrow band implies little dependence of fractional yields on p , as expected. A formal expression of the theoretical fractional yield is shown in Appendix D.

An inspection of Figs. 12 and 13 discloses that empirical, inferred from Eqs. (14) and (18), and theoretical fractional yields are consistent (in the sense that horizontal bars related to the former lie between vertical bands related to the latter) only for Na and Na, Mg, Si, Ca, Ni (leaving aside KD population), respectively, while the contrary holds for the remaining elements. The discrepancy could be due to a number of reasons, for instance (i) subsamples are poorly populated and different regression lines might be related to richer subsamples; (ii) Ti, Cr, Fe, (at least) are appreciably synthesised outside SNII progenitors e.g., SNIa progenitors and AGB stars; (iii)

updated models make O production reduced by a factor of about 2 and Ti, Cr, Fe production increased by a comparable factor; (iv) lower empirical fractional yields are expected in presence of significant cosmic scatter provided it is more efficient for light elements with respect to heavy elements.

The substitution of Eq. (18) into (14) produces:

$$b_Q = \log \frac{\alpha_O}{\alpha_Q} ; \quad (19)$$

which is the intercept of the straight line, expressed by Eq. (1), inferred from the data in the light of simple MCBR models, implying $a_Q = 1$ via Eq. (2). Values of intercept, b_Q , and related rms error, σ_{b_Q} , expressed by Eqs. (19), (38), are listed in Table 5. The comparison with their counterparts, listed in Table 1, shows results consistent within $\mp 2\sigma_{b_Q}$ or less, for assigned element, Q, and subsample, LH, HH, KD, HA.

The straight lines of unit slope and intercept, inferred from Eq. (19), are plotted in Figs. 14 and 15 for $Q = \text{Na, Mg, Si, Ca}$, and $Q = \text{Ti, Cr, Fe, Ni}$, respectively, and compared to the data. The above mentioned lines are consistent with the main sequences enclosing the data, shown in Figs. 1 and 2, within $\mp 2\sigma_{b_Q}$ or less.

The cut parameter (ratio of element abundance within the flowing gas to its counterpart within the pre-existing gas), ζ_Q , in the case under discussion is expressed as (Caimmi 2011a, 2012a):

$$\zeta_Q = 1 - \frac{A_Q \hat{p}_Q}{\kappa} ; \quad A_Q = \frac{Z_\odot}{(Z_Q)_\odot} ; \quad (20)$$

where Z is the total metal abundance. The substitution of Eq. (17) into (20) after some algebra yields:

$$\zeta_Q = 1 + \frac{Z_\odot}{\ln 10} \frac{1}{\alpha_Q} \frac{1 + \kappa}{\kappa} ; \quad (21)$$

in the limit of strong outflow, $\kappa \gg 1$, $\alpha_Q \ll -1$, which implies $\zeta_Q \lesssim 1$, as expected.

With regard to a selected element, Q, the assumption of a universal stellar initial mass function implies constant yield, \hat{p}_Q , for different populations, P1 and P2 say. Accordingly, the following relation is inferred from Eq. (17):

$$\frac{(\alpha_Q)_{P1}}{(\alpha_Q)_{P2}} = \frac{1 + \kappa_{P1}}{1 + \kappa_{P2}} ; \quad (22)$$

where the ratio on the right-hand side may be conceived as an indicator of the flow parameter ratio between the populations, P1 and P2; $Pi = \text{LH, HH, KD}$,

HA, $i = 1, 2$. Computed values, $(F_Q)_{XY} = (\alpha_Q)_{XY}/(\alpha_Q)_{LH}$, together with related rms errors, $\sigma_{(F_Q)_{XY}} = \sigma_{(\alpha_Q)_{XY}}/(\alpha_Q)_{LH}$, expressed by Eq. (34), assumed lower and upper limit, $(F_Q)_{XY}^{\mp} = (\alpha_Q)_{XY}/(\alpha_Q)_{LH} \mp 2\sigma_{(\alpha_Q)_{XY}}/(\alpha_Q)_{LH}$, for Q = O, Na, Mg, Si, Ca, Ti, Cr, Fe, Ni; P1 = HH, KD, HA; P2 = LH; are listed in Table 6.

For an assigned population, the flow parameter, κ , must necessarily remain unchanged for different elements. The intersection of assumed validity ranges, $(F_Q)_{XY}^{\mp} = (F_Q)_{XY} \mp 2\sigma_{(F_Q)_{XY}}$, is denoted as \cap_Q and related values (mean, semiamplitude, lower and upper limit) are listed for each case in the bottom panel of Table 6. The last results disclose that, with respect to LH population environment, HH, KD, HA population environments were characterized by an outflow to star formation rate ratio lower than about 30%, 53%, 37%, respectively.

The above considerations hold within the framework of simple MCBR models of chemical evolution, which imply (among others) the assumption of instantaneous mixing. An opposite extreme situation may be the following: chemical enrichment took place before sample stars were formed, then abundance differences are entirely due to cosmic scatter. If cosmic scatter obeys a Gaussian distribution where the mean and the variance can be evaluated from the data, the theoretical differential abundance distribution reads (Caimmi 2013):

$$(\psi)_{cs} = \log \left\{ \frac{1}{\ln 10} \frac{1}{\sqrt{2\pi}\sigma_Q} \exp \left[-\frac{(\log -\overline{\log \phi_Q})^2}{2\sigma_Q^2} \right] \frac{1}{\phi_Q} \right\} ; \quad (23)$$

where the index, cs, denotes cosmic scatter, $\overline{\log \phi_Q} = [\overline{Q/H}]$ and $\sigma_Q = \sigma_{[Q/H]}$. Related curves, expressed by Eq. (23), are plotted in Figs. 3-11 for Q = O, Na, Mg, Si, Ca, Ti, Cr, Fe, Ni, with regard to LH, HH, KD, HA subsamples. An inspection of Figs. 3-11, leaving aside bins populated by a single star when appropriate, discloses the following.

- (1) The declining part of the distribution, covering a metallicity range where most data lie, is slightly different from a straight line.
- (2) The rising part of the distribution, in principle, offers a natural solution to the FGK-dwarf problem.
- (3) The distribution (full curve) fits to the data to a comparable extent with respect to simple MCBR models (dashed straight line) with a slight preference for the last alternative in a few cases, for LH, HH, KD subsamples. The same holds for HA subsample, with the exception of O, Si, Ca, where a marked preference towards chemical evolution, within the framework of simple MCBR models, can be recognized.

Table 6: Slope ratio, $(F_Q)_{XY} = (\alpha_Q)_{XY}/(\alpha_Q)_{LH}$, related rms error, $\sigma_{(F_Q)_{XY}}$, assumed lower and upper limit, $(F_Q)_{XY}^{\mp} = (F_Q)_{XY} \mp 2\sigma_{(F_Q)_{XY}}$, for different elements, $Q = O, Na, Mg, Si, Ca, Ti, Cr, Fe, Ni$, and different subsamples, $XY = HH, KD, HA$. With regard to lower limits, $(F_Q)_{XY}^-$, unphysical negative values are replaced by null values. The intersection of assumed validity ranges, $(F_Q)_{XY}^{\mp} = (F_Q)_{XY} \mp 2\sigma_{(F_Q)_{XY}}$, is denoted as \cap_Q and related values (mean, semiamplitude, lower and upper limit) are listed for each case in the lower panel. See text for further details.

| Q | XY | $(F_Q)_{XY}$ | $\sigma_{(F_Q)_{XY}}$ | $(F_Q)_{XY}^-$ | $(F_Q)_{XY}^+$ |
|----------|----|--------------|-----------------------|----------------|----------------|
| O | HH | 0.3871 | 0.1851 | 0.0169 | 0.7573 |
| | KD | 1.2899 | 0.4445 | 0.4009 | 2.1789 |
| | HA | 0.3799 | 0.1919 | 0 | 0.7637 |
| Na | HH | 0.2723 | 0.1315 | 0.0093 | 0.5353 |
| | KD | 0.3776 | 0.1424 | 0.0928 | 0.6624 |
| | HA | 0.2477 | 0.1057 | 0.0363 | 0.4591 |
| Mg | HH | 0.2880 | 0.1010 | 0.0860 | 0.4900 |
| | KD | 0.5811 | 0.1720 | 0.2371 | 0.9251 |
| | HA | 0.2824 | 0.1264 | 0.0296 | 0.5352 |
| Si | HH | 0.1979 | 0.0925 | 0.0129 | 0.3829 |
| | KD | 0.3853 | 0.1420 | 0.1013 | 0.6693 |
| | HA | 0.1979 | 0.0925 | 0.0129 | 0.3829 |
| Ca | HH | 0.4034 | 0.2314 | 0 | 0.8662 |
| | KD | 1.0722 | 0.5604 | 0 | 2.1930 |
| | HA | 1.0704 | 0.6017 | 0 | 2.2738 |
| Ti | HH | 0.5058 | 0.2684 | 0 | 1.0426 |
| | KD | 1.1454 | 0.6188 | 0 | 2.3830 |
| | HA | 0.7058 | 0.4057 | 0 | 1.5172 |
| Cr | HH | 0.5121 | 0.1503 | 0.2115 | 0.8127 |
| | KD | 0.8363 | 0.2753 | 0.2857 | 1.3869 |
| | HA | 0.7249 | 0.1887 | 0.3475 | 1.1023 |
| Fe | HH | 0.6313 | 0.2721 | 0.0871 | 1.1755 |
| | KD | 0.7726 | 0.4404 | 0 | 1.6534 |
| | HA | 0.5616 | 0.3245 | 0 | 1.2106 |
| Ni | HH | 0.3603 | 0.1465 | 0.0673 | 0.6533 |
| | KD | 0.5804 | 0.1359 | 0.3086 | 0.8522 |
| | HA | 0.3585 | 0.1305 | 0.0975 | 0.6195 |
| \cap_Q | HH | 0.2972 | 0.0852 | 0.2115 | 0.3829 |
| | KD | 0.5317 | 0.1308 | 0.4009 | 0.6625 |
| | HA | 0.3652 | 0.0177 | 0.3475 | 0.3829 |

In conclusion, both instantaneous mixing (in the framework of MCBR models) and cosmic scatter offer viable interpretations to the data, provided HH and KD populations underwent distinct chemical evolution, as suggested by a recent investigation (Ishigaki et al. 2013). If the contrary holds and HA population is considered, then instantaneous mixing in presence of chemical evolution is preferred with respect to cosmic scatter in absence of chemical evolution.

Different kinematical trends have been recently found for LH, HH, KD populations. More specifically, LH stars show larger Galactocentric distance components on both the equatorial plane and the polar axis, with respect to HH and KD stars. Accordingly, LH and HH stars may be conceived as requiring different formation scenarios, with LH stars being accreted. For further details refer to the parent paper (Schuster et al. 2012).

Lower $[\text{O}/\text{Fe}]$ values shown by LH stars with respect to HH stars may be explained in different ways according if the variation is in $[\text{O}/\text{H}]$ or in $[\text{Fe}/\text{H}]$ or both. Lower $[\text{O}/\text{H}]$ values in LH stars could be related to oxygen depletion in second generation stars within globular clusters, while higher $[\text{Fe}/\text{H}]$ values could be related to the contribution from SNIa explosions and subsequent star formation, regardless of the birth place. In both cases, HH population appears to be older than LH population, which implies similar kinematical trends if the above mentioned populations formed in situ, contrary to current data (Ra12).

An interpretation in the framework of the secondary infall scenario could be the following. The environment of HH population is related to the inner and denser region of the proto-Galaxy, which first virialized while the external shells were still expanding. The environment of LH population is related to the outer and less dense region of the proto-Galaxy, which virialized at a later epoch and probably mixed with SNIa ejecta before forming the first star generation.

5 Conclusion

A linear $[\text{Q}/\text{H}]-[\text{O}/\text{H}]$ relation has been inferred from different populations sampled in recent attempts (NS10; Ra12), namely LH (low- α halo stars, $N = 24$); HH (high- α halo stars, $N = 25$); KD (thick disk stars, $N = 16$); for $\text{Q} = \text{Na}, \text{Mg}, \text{Si}, \text{Ca}, \text{Ti}, \text{Cr}, \text{Fe}, \text{Ni}$.

The empirical, differential element abundance distribution has been determined for different populations together with related theoretical counterpart within the framework of simple MCBR models. Fractional yields have been inferred from the data in the framework of simple MCBR models, includ-

ing an example of comparison with theoretical counterparts deduced from SNII progenitor nucleosynthesis for solar and subsolar metallicity, under the assumption of power-law stellar initial mass function.

Regardless of the chemical evolution model, fractional generalized yields have been determined. The ratio of outflow to star formation rate has been evaluated for a selected population with respect to a reference one.

The theoretical, differential element abundance distribution has been inferred from the data for different populations, in the opposite limit of inhomogeneous mixing due to cosmic scatter obeying a Gaussian distribution whose mean and variance have been evaluated from the related subsample.

The main results may be summarized as follows.

- (1) With regard to the $(O[O/H][Q/H])$ plane, stars display along a “main sequence”, $[Q, O] = [a_Q, b_Q, \Delta b_Q]$, in connection with the straight line, $[Q/H] = a_Q[O/H] + b_Q$. For unit slopes, $a_Q = 1$, a main sequence relates to constant $[O/Q]$ abundance ratio. In most cases (e.g., Na) stars from OL subsample (two globular cluster outliers) lie outside the main sequence.
- (2) Regardless of the population, regression line slope estimators fit to the unit slope within $\pm 2\hat{\sigma}_{a_Q}$ for Mg, Si, Ti; within $\pm 3\hat{\sigma}_{a_Q}$ for Cr, Fe, Ni; within $\pm r\hat{\sigma}_{a_Q}$, $r > 3$, for Ca, Na; where the fit to the unit slope implies related elements are simple primary i.e. synthesised within SNII progenitors in presence of universal stellar initial mass function.
- (3) Within the framework of simple MCBR chemical evolution models (Caimmi 2011a; 2012a), fractional yields are consistent with theoretical results from SNII progenitor nucleosynthesis (Woosley and Weaver 1995) for Na, Mg, Si, Ca, Ni (with the exception of KD population) while the contrary holds for Ti, Cr, Fe, where theoretical values appear to be underestimated but the contribution from SNIa progenitors could fill the gap.
- (4) Within the framework of simple MCBR models, a ratio of outflow to star formation rate has been inferred, of about 30%, 53%, 37%, for HH, KD, HA population environment, respectively, in comparison with LH population environment.
- (5) Theoretical, differential element abundance distributions due to cosmic scatter obeying a Gaussian distribution, fit to the data to a comparable extent with respect to its counterpart within the framework of simple MCBR models, for LH, HH, KD population, while the last alternative

is preferred for HA population provided the inner halo and the thick disk underwent common chemical evolution.

Acknowledgement

Thanks are due to the referee, S. Ninković, for critical comments which improved an earlier version of the current paper.

References

- [1] Asplund, M., Grevesse, N., Sauval, A.J., Scott, P.: 2009, *Ann. Rev. Astron. Astrophys.*, 47, 481.
- [2] Caimmi, R.: 2007, *New Astron.*, 12, 289.
- [3] Caimmi, R.: 2011a, *Ser. Astron. J.*, 183, 37.
- [4] Caimmi, R.: 2011b, *New Astron.*, 16, 337.
- [5] Caimmi, R.: 2012a, *Ser. Astron. J.*, 185, 35.
- [6] Caimmi, R.: 2012b, *Intellectual Archive*, 1, 71, ISSN 1929-4700 Toronto. (arxiv 1111.2680).
- [7] Caimmi, R.: 2013, *Ser. Astron. J.*, 186, 25.
- [8] Carretta, E.: 2006, *Astron. J.*, 131, 1766.
- [9] Carretta, E.: 2013, *Astron. Astrophys.*, 557, A128.
- [10] Carretta, E., Bragaglia, A., Gratton, R. G., Lucatello, S., Momany, Y.: 2007a, *Astron. Astrophys.*, 464, 927.
- [11] Carretta, E., Bragaglia, A., Gratton, R. G., et al.: 2007b, *Astron. Astrophys.*, 464, 939.
- [12] Carretta, E., Bragaglia, A., Gratton, R., Lucatello, S.: 2009a, *Astron. Astrophys.*, 505, 139.
- [13] Carretta, E., Bragaglia, A., Gratton, R. G., et al.: 2009b, *Astron. Astrophys.*, 505, 117.
- [14] Carretta, E., Bragaglia, A., Gratton, R. G., et al.: 2010, *Astrophys. J.*, 714, L7.

- [15] Conroy, C.: 2012, *Astrophys. J.*, 758, 21.
- [16] Edvardsson, B., Andersen, J., Gustaffson, B., et al.: 1993, *Astron. Astrophys.*, 275, 101.
- [17] Fulbright, J.P.: 2002, *Astron. J.*, 123, 404.
- [18] Gratton, R.G., Carretta, E., Desidera, S., Lucatello, S., Mazzei, P., Barbieri, M., 2003. *Astron. Astrophys.*, 406, 131.
- [19] Gratton, R.G., Lucatello, S., Bragaglia, A., et al.: 2007, *Astron. Astrophys.*, 464, 953.
- [20] Ishigaki, M.N., Aoki, W., Chiba, M.: 2013, *Astrophys. J.*, 771, 67.
- [21] Isobe, T., Feigelson, E.D., Akritas, M.G., Babu, G.J.: 1990, *Astrophys. J.*, 364, 104.
- [22] Kobayashi, C., Tsujimoto, T., Nomoto, K., Hachisu, I., Kato, M., 1998. *Astrophys. J.* 503, L155.
- [23] Kobayashi, C., Nomoto, K., 2009. *Astrophys. J.* 707, 1466.
- [24] Kobayashi, C., Karakas, A. I., Umeda, H., 2011. *Mont. Not. R. Astron. Soc.* 414, 3231.
- [25] Johnson, C. I., Pilachowski, C. A.: 2012, *Astrophys. J.*, 754, L38.
- [26] McWilliam, A., 1997. *Ann. Rev. Astron. Astrophys.* 35, 503.
- [27] Nissen, P.E., Schuster, W.J.: 1997, *Astron. Astrophys.*, 326, 751.
- [28] Nissen, P.E., Schuster, W.J.: 2010, *Astron. Astrophys.*, 511, L10. (NS10).
- [29] Pagel, B. E. J., Tautvaisiene, G.: 1995, *Mon. Not. R. Astron. Soc.*, 276, 505.
- [30] Ramírez, I., Meléndez, J., Chanamé, J.: 2012, *Astrophys. J.*, 757, 164. (Ra12).
- [31] Schuster, W.J., Moreno, E., Nissen, P. E., Pichardo, B.: 2012, *Astron. Astrophys.*, 538, A21.
- [32] Stephens, A., Boesgaard, A. M.: 2002, *Astron. J.*, 123, 1647.

- [33] Timmes, F. X., Woosley, S. E., Weaver, T. A., 1995. *Astrophys. J. Supp.* 98, 617.
- [34] Venn, K.A., Irwin, M., Shetrone, M.D., Tout, C.A.; Hill, V., Tolstoy, E., 2004. *Astron. J.* 128, 1177.
- [35] Wallerstein, G., Iben, I., Parker, P., et al., 1997. *Rev. Mod. Phys.* 69, 995.
- [36] Wheeler, J. C., Sneden, C., Truran, J. W., 1989. *Ann. Rev. Astron. Astrophys.* 27, 279.
- [37] Woosley, S. E., Weaver, T. A., 1995. *Astrophys. J. Supp.* 101, 181.

Appendix

A Solar photospheric mass abundances

Solar photospheric mass abundances may be inferred from the following general relations:

$$Z_Q = \frac{M_Q}{M} = \frac{M_Q}{M_H} \frac{M_H}{M} = \frac{N_Q \bar{m}_Q}{N_H \bar{m}_H} X \quad ; \quad (24)$$

$$\mathcal{Q} = 12 + \log \left(\frac{N_Q}{N_H} \right) \quad ; \quad (25)$$

$$\frac{\bar{m}_Q}{\bar{m}_H} = \frac{\sum_k P_{Q_k} m_{Q_k}}{\sum_j P_{H_j} m_{H_j}} = \frac{\sum_k P_{Q_k} A_{Q_k}}{\sum_j P_{H_j} A_{H_j}} \quad ; \quad (26)$$

where \bar{m}_Q is the mean atomic mass of the element, Q , in units of the proton mass, m_p ; \mathcal{Q} is an indicator of the fractional number abundance of the element, Q , with respect to hydrogen; P_{Q_k} is the fractional abundance of the isotopic species, Q_k ($Q = H$ for hydrogen), $\sum_k P_{Q_k} = 1$; A_{Q_k} is the mass number of the isotopic species, Q_k . The result is:

$$\frac{(Z_Q)_\odot}{X_\odot} = \exp_{10}(\mathcal{Q} - 12) \frac{\sum_k P_{Q_k} A_{Q_k}}{\sum_j P_{H_j} A_{H_j}} \quad ; \quad (27)$$

which can be inserted into Eq. (10). The results for the solar photospheric mass abundances, Z_Q , $Q = O, Na, Mg, Si, Ca, Ti, Cr, Fe, Ni$, are listed in Table 7. Related values for helium and metals are $Y = Z_{He} = 0.2485$ and $Z = \sum_{Q \neq H, He} Z_Q = 0.0134$, respectively (Asplund et al. 2009).

Table 7: Solar photospheric mass abundances, Z_Q , inferred from number abundance indicators, \mathcal{Q} (normalized to $\mathcal{H} = 12$), and isotopic abundance fractions of the solar photosphere determined in a recent investigation (Asplund et al. 2009, Tables 1, 3, 4, therein). Hydrogen abundance, $Z_H = X$, is necessary for evaluating Z_Q , $Q \neq H$, according to Eq. (27). The atomic number is denoted as \mathcal{Z} . For further details refer to the text.

| \mathcal{Z} | Q | \mathcal{Q} | Z_Q |
|---------------|----|---------------|----------|
| 1 | H | 12.00 | 7.381E-1 |
| 8 | O | 8.69 | 5.786E-3 |
| 11 | Na | 6.24 | 2.950E-5 |
| 12 | Mg | 7.60 | 7.146E-4 |
| 14 | Si | 7.51 | 6.713E-4 |
| 20 | Ca | 6.34 | 6.478E-5 |
| 22 | Ti | 4.95 | 3.152E-6 |
| 24 | Cr | 5.64 | 1.677E-5 |
| 26 | Fe | 7.50 | 1.305E-3 |
| 28 | Ni | 6.22 | 7.198E-5 |

B Fractional yields in simple MCBR models

With regard to simple MCBR chemical evolution models (Caimmi 2011a; 2012), the combination of Eqs. (11) and (12) yields:

$$\frac{\phi_Q - (\phi_Q)_i}{\phi_O - (\phi_O)_i} = \frac{(Z_O)_\odot \hat{p}_Q}{(Z_Q)_\odot \hat{p}_O} ; \quad (28)$$

where, on the other hand, an assumption of the model is $Z = c_Q Z_Q = c_O Z_O$, Z global fractional metal mass abundance, c_Q and c_O constant, (Caimmi 2011a), which via Eq. (7) is equivalent to:

$$\frac{\phi_Q}{\phi_O} = \frac{(\phi_Q)_i}{(\phi_O)_i} = \frac{c_O (Z_O)_\odot}{c_Q (Z_Q)_\odot} ; \quad (29)$$

provided Q and O are simple primary elements.

Starting from $Z - Z_i = c_Q [Z_Q - (Z_Q)_i] = c_O [Z_O - (Z_O)_i]$ and following the same way yields:

$$\frac{\phi_Q - (\phi_Q)_i}{\phi_O - (\phi_O)_i} = \frac{c_O (Z_O)_\odot}{c_Q (Z_Q)_\odot} ; \quad (30)$$

and the combination of Eqs. (29) and (30) produces:

$$\frac{\phi_Q - (\phi_Q)_i}{\phi_O - (\phi_O)_i} = \frac{\phi_Q}{\phi_O} ; \quad (31)$$

which implies $\phi_Q/\phi_O = (\phi_Q)_i/(\phi_O)_i$, as expected.

Finally, the substitution of Eq. (31) into (28) yields Eq. (13).

C Fractional yield, intercept and fractional slope uncertainties

Fractional yield, intercept and fractional slope uncertainties, mentioned in the text, are evaluated using standard formulae of error propagation. Though only quadratic errors have been used in the current attempt, for sake of completeness also absolute errors shall be included in the following.

Let m_1, m_2, \dots, m_v , be independent random variables obeying Gaussian distributions and let m be a random variable which depends on m_1, m_2, \dots, m_v , as $m = f(m_1, m_2, \dots, m_v)$, where f is a specified continuous and derivable function. According to a theorem of statistics, related quadratic and absolute errors read:

$$\sigma_m = \left\{ \sum_{r=1}^v \left[\left(\frac{\partial f}{\partial m_r} \right)_{P^*} \sigma_{m_r} \right]^2 \right\}^{1/2} ; \quad (32)$$

$$\Delta m = \sum_{r=1}^v \left| \left(\frac{\partial f}{\partial m_r} \right)_{P^*} \right| \Delta m_r ; \quad (33)$$

where $P^* \equiv (m_1^*, m_2^*, \dots, m_v^*)$, m_r^* is the expected value (approximated by the mean) of the distribution depending on m_r , σ_{m_r} the related rms error (approximated by the rms deviation), Δm_r the maximum error (in absolute value) on the determination of m_r .

The particularization of Eqs. (32), (33), to the fractional yield, \hat{p}_Q/\hat{p}_O , expressed by Eq. (14), after some algebra yields:

$$\sigma_{\hat{p}_Q/\hat{p}_O} = \frac{\hat{p}_Q}{\hat{p}_O} \frac{\sigma_{b_Q}}{\ln 10} ; \quad (34)$$

$$\Delta \frac{\hat{p}_Q}{\hat{p}_O} = \frac{\hat{p}_Q}{\hat{p}_O} \frac{\Delta b_Q}{\ln 10} ; \quad (35)$$

where σ_{b_Q} , Δb_Q , can be inferred from Table 1.

The particularization of Eqs. (32), (33), to the fractional yield, \hat{p}_Q/\hat{p}_O , expressed by Eq. (18), after some algebra yields:

$$\sigma_{\hat{p}_Q/\hat{p}_O} = \frac{\hat{p}_Q}{\hat{p}_O} \left[\left(\frac{\sigma_{\alpha_O}}{\alpha_O} \right)^2 + \left(\frac{\sigma_{\alpha_Q}}{\alpha_Q} \right)^2 \right]^{1/2} ; \quad (36)$$

$$\Delta \frac{\hat{p}_Q}{\hat{p}_O} = \frac{\hat{p}_Q}{\hat{p}_O} \left[\left| \frac{\Delta \alpha_O}{\alpha_O} \right| + \left| \frac{\Delta \alpha_Q}{\alpha_Q} \right| \right] ; \quad (37)$$

where σ_{α_Q} , $\Delta \alpha_Q$, can be inferred from Table 2.

The particularization of Eqs. (32), (33), to the intercept, b_Q , expressed by Eq. (19), after some algebra yields:

$$\sigma_{b_Q} = \frac{1}{\ln 10} \left[\left(\frac{\sigma_{\alpha_O}}{\alpha_O} \right)^2 + \left(\frac{\sigma_{\alpha_Q}}{\alpha_Q} \right)^2 \right]^{1/2} ; \quad (38)$$

$$\Delta b_Q = \frac{1}{\ln 10} \left[\left| \frac{\Delta \alpha_O}{\alpha_O} \right| + \left| \frac{\Delta \alpha_Q}{\alpha_Q} \right| \right] ; \quad (39)$$

where σ_{α_Q} , $\Delta \alpha_Q$, can be inferred from Table 2.

The particularization of Eqs. (32), (33), to the fractional slope, $(\alpha_Q)_{P1}/(\alpha_Q)_{P2}$, after some algebra yields:

$$\sigma_{(\alpha_Q)_{P1}/(\alpha_Q)_{P2}} = \frac{(\alpha_Q)_{P1}}{(\alpha_Q)_{P2}} \left[\left(\frac{(\sigma_{\alpha_Q})_{P1}}{(\alpha_Q)_{P1}} \right)^2 + \left(\frac{(\sigma_{\alpha_Q})_{P2}}{(\alpha_Q)_{P2}} \right)^2 \right]^{1/2} ; \quad (40)$$

$$\Delta \frac{(\alpha_Q)_{P1}}{(\alpha_Q)_{P2}} = \frac{(\alpha_Q)_{P1}}{(\alpha_Q)_{P2}} \left[\left| \frac{\Delta(\alpha_Q)_{P1}}{(\alpha_Q)_{P1}} \right| + \left| \frac{\Delta(\alpha_Q)_{P2}}{(\alpha_Q)_{P2}} \right| \right] ; \quad (41)$$

where $\sigma_{(\alpha_Q)_{Pi}}$, $\Delta(\alpha_Q)_{Pi}$, $i = 1, 2$, can be inferred from Table 2.

D Fractional yields from star nucleosynthesis

Let $\Delta(m_i)_Q$ be the mass in the element, Q, synthesised within a star of initial mass, m_i , $1 \leq i \leq n$, and returned to the interstellar medium after star death, for which the result is known. The restriction of a linear trend between contiguous values, m_j , m_{j+1} , $1 \leq j \leq n - 1$, reads:

$$\frac{\Delta m_Q - \Delta(m_j)_Q}{\Delta(m_{j+1})_Q - \Delta(m_j)_Q} = \frac{m - m_j}{m_{j+1} - m_j} ; \quad (42)$$

where $m_j \leq m \leq m_{j+1}$ without loss of generality.

The straight line, defined by Eq. (42), takes the expression:

$$\Delta m_Q = (A_j)_Q m + (B_j)_Q m_\odot ; \quad (43)$$

$$(A_j)_Q = \frac{\Delta(m_{j+1})_Q - \Delta(m_j)_Q}{m_{j+1} - m_j} ; \quad (44)$$

$$(B_j)_Q = \frac{\Delta(m_j)_Q}{m_\odot} - (A_j)_Q \frac{m_j}{m_\odot} ; \quad (45)$$

where masses are expressed in solar units.

The further restriction of a power-law stellar initial mass function:

$$\phi\left(\frac{m}{m_\odot}\right) = C\left(\frac{m}{m_\odot}\right)^{-p} ; \quad (46)$$

where C is a normalization constant and $-p$ the power-law exponent, allows a simple expression for the mass in the element, Q, synthesised within stars of initial mass, $m_j \leq m \leq m_{j+1}$, $1 \leq j \leq n-1$, and returned to the interstellar medium after star death.

The result is:

$$\Delta_j m_Q = \int_{m_j/m_\odot}^{m_{j+1}/m_\odot} \Delta m_Q \phi\left(\frac{m}{m_\odot}\right) d\left(\frac{m}{m_\odot}\right) ; \quad (47)$$

and the substitution of Eqs. (43)-(46) into (47) after some algebra yields:

$$\begin{aligned} \Delta_j m_Q = C m_\odot \left\{ \frac{(A_j)_Q}{2-p} \left[\left(\frac{m_{j+1}}{m_\odot}\right)^{2-p} - \left(\frac{m_j}{m_\odot}\right)^{2-p} \right] \right. \\ \left. + \frac{(B_j)_Q}{1-p} \left[\left(\frac{m_{j+1}}{m_\odot}\right)^{1-p} - \left(\frac{m_j}{m_\odot}\right)^{1-p} \right] \right\} ; \quad (48) \end{aligned}$$

where the power-law exponent may safely be assumed as lying within the range, $-3 \leq -p \leq -2$.

The mass in the element, Q, synthesised within the whole stellar generation (sg) and returned to the interstellar medium after star death, is:

$$\Delta_{sg} m_Q = \sum_{j=1}^{n-1} \Delta_j m_Q ; \quad (49)$$

where, after substitution of Eq. (48) into (49), m_1 and m_n are the lower and upper mass limit, respectively, of stars which produce and, when dying, return the element, Q, to the interstellar medium.

In the framework of simple MCBR models, the yield of the element, Q , can be expressed as (e.g., Caimmi 2007):

$$\hat{p}_Q = \frac{I_Q(12)}{\alpha I(1)} \quad ; \quad (50)$$

where $I_Q(12) = \Delta_{\text{sg}} m_Q$ and $\alpha, I(1)$, are independent of Q . Accordingly, the fractional yield related to selected elements, Q_1, Q_2 , reads:

$$\frac{\hat{p}_{Q_1}}{\hat{p}_{Q_2}} = \frac{\Delta_{\text{sg}} m_{Q_1}}{\Delta_{\text{sg}} m_{Q_2}} \quad ; \quad (51)$$

where the substitution of Eqs. (48) and (49) into (51) implies the disappearance of the product, Cm_\odot .

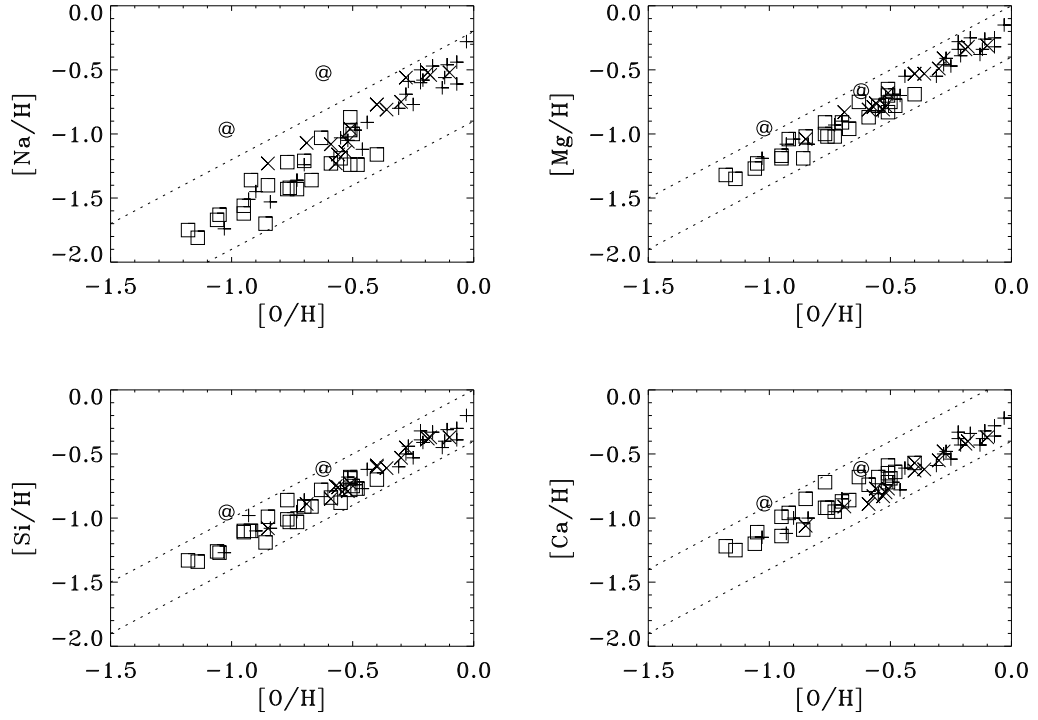


Figure 1: The empirical $[Q/H]$ - $[O/H]$ relation, $Q = \text{Na, Mg, Si, Ca}$, for subsamples, LH (low- α halo stars, open squares), HH (high- α halo stars, crosses), KD (low-metallicity thick disk stars, saltires), OL (globular cluster outliers, “at” symbols). Also shown for comparison is the narrowest “main sequence”, $[Q,O] = [1, b_Q, \Delta b_Q]$, within which the data lie leaving outside OL stars. Typical error bars are about twice the symbol dimensions. See text for further details.

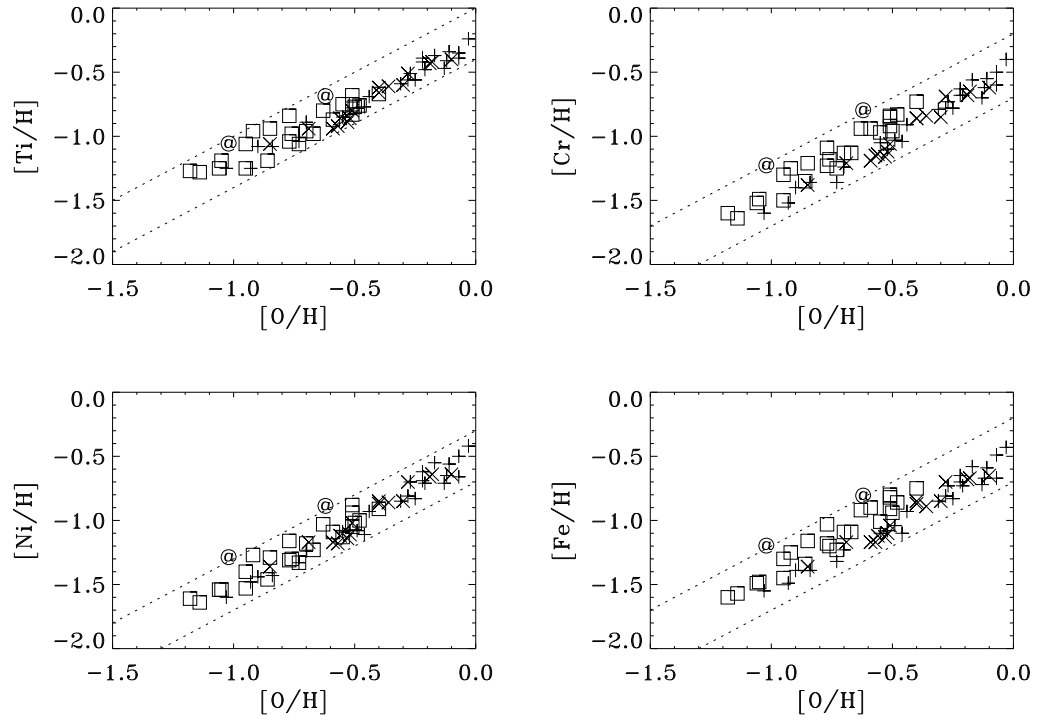


Figure 2: As in Fig. 1, but for $Q = \text{Ti, Cr, Fe, Ni}$.

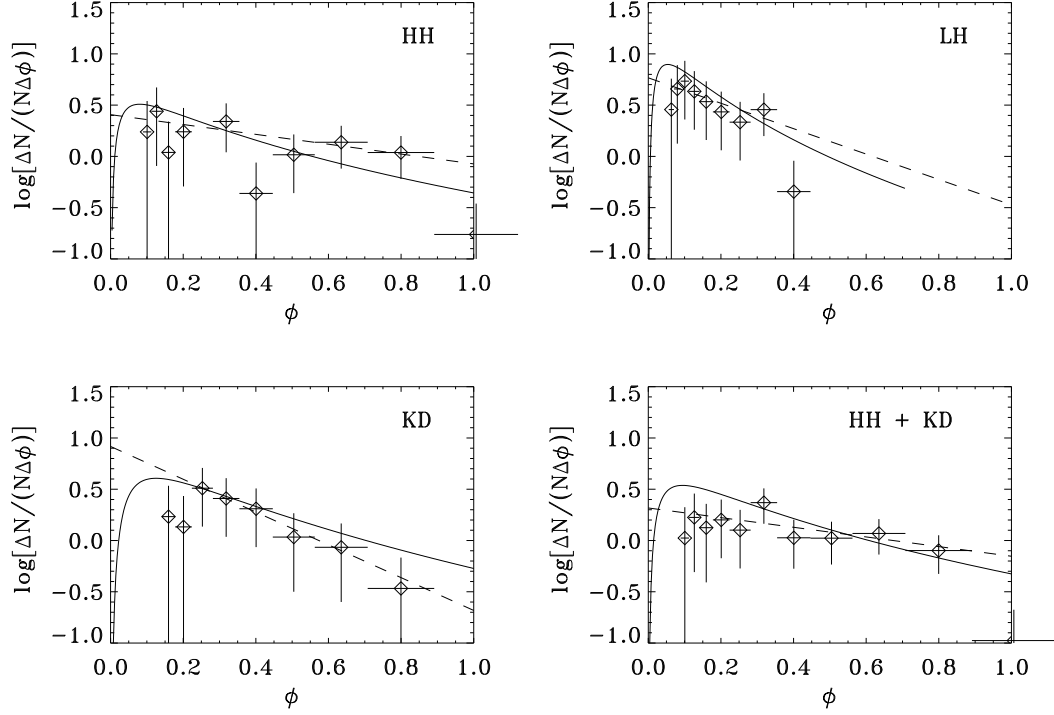


Figure 3: The empirical differential oxygen abundance distribution inferred from HH, LH, KD, HA = HH + KD subsamples. Lower uncertainties attaining the horizontal axis (decreasing up to negative infinity) relate to bins populated by a single star. Dashed straight lines represent regression lines to points defining bins populated by at least two stars. Full curves represent the theoretical differential oxygen distribution due to intrinsic scatter obeying a Gaussian distribution with mean and variance inferred from the data. See text for further details.

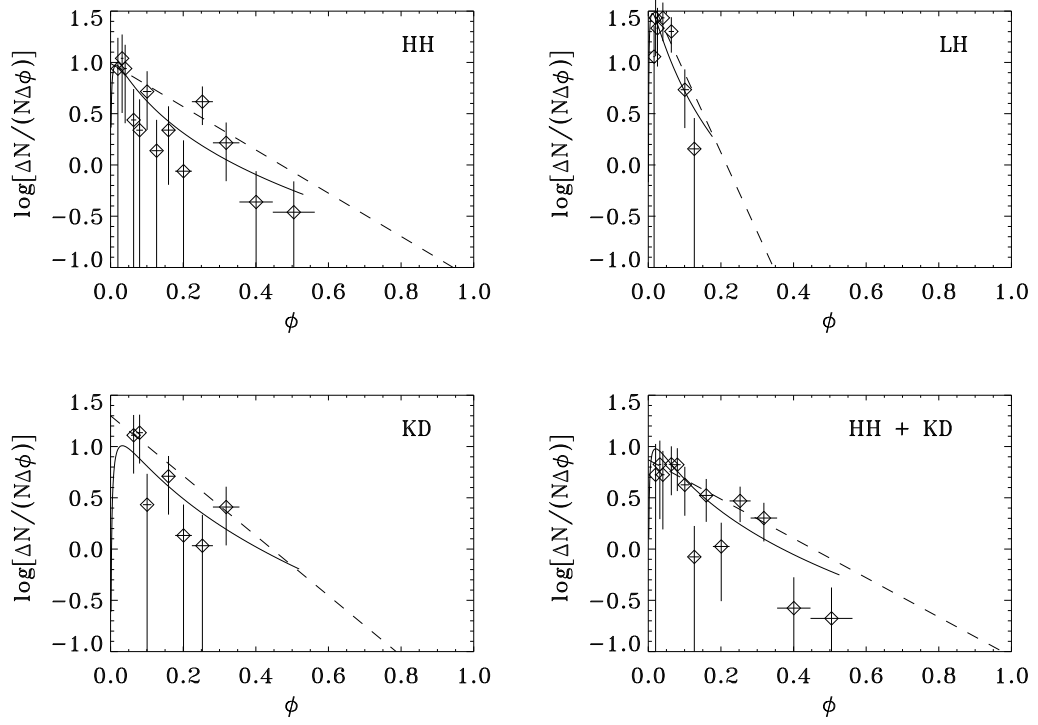


Figure 4: As in Fig. 3, but concerning sodium instead of oxygen.

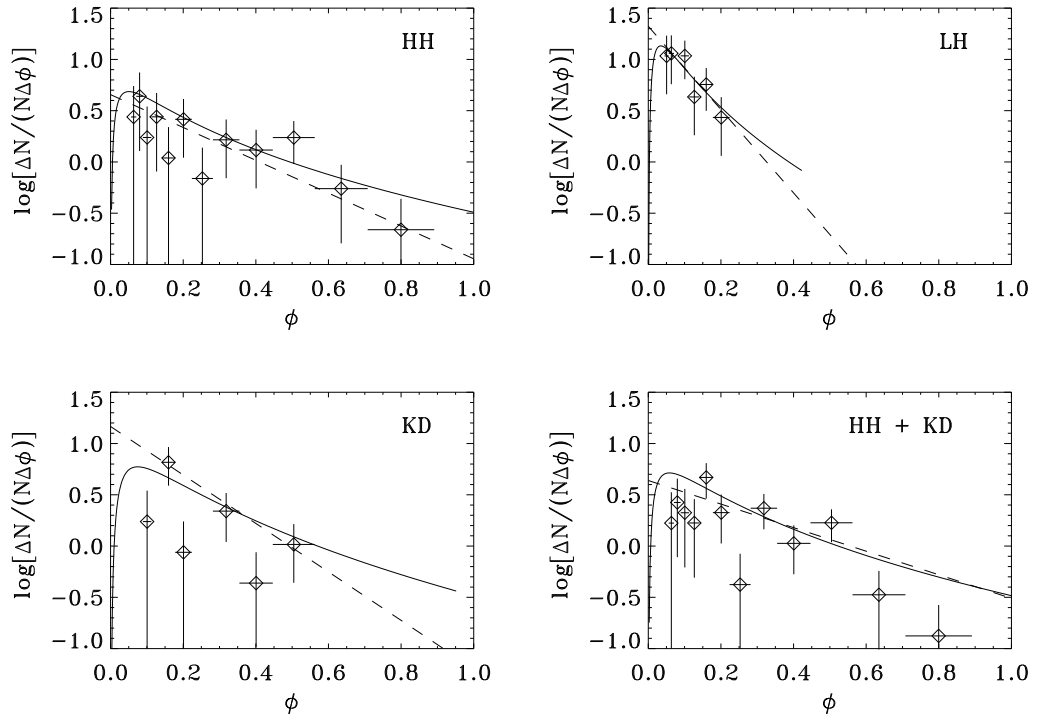


Figure 5: As in Fig. 3, but concerning magnesium instead of oxygen.

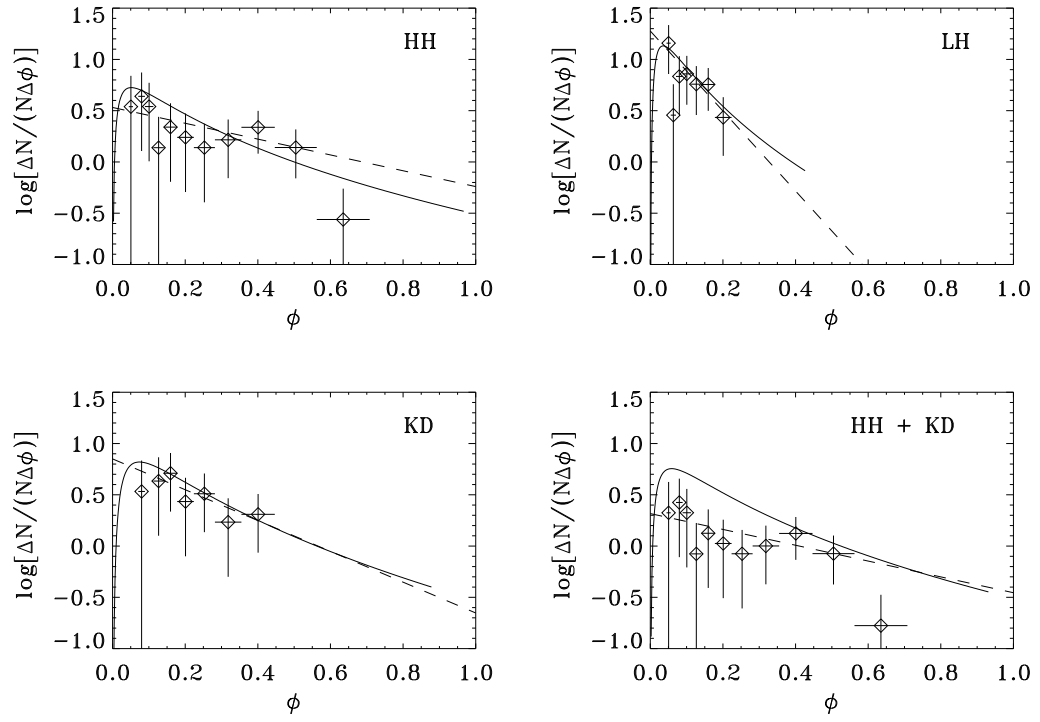


Figure 6: As in Fig. 3, but concerning silicon instead of oxygen.

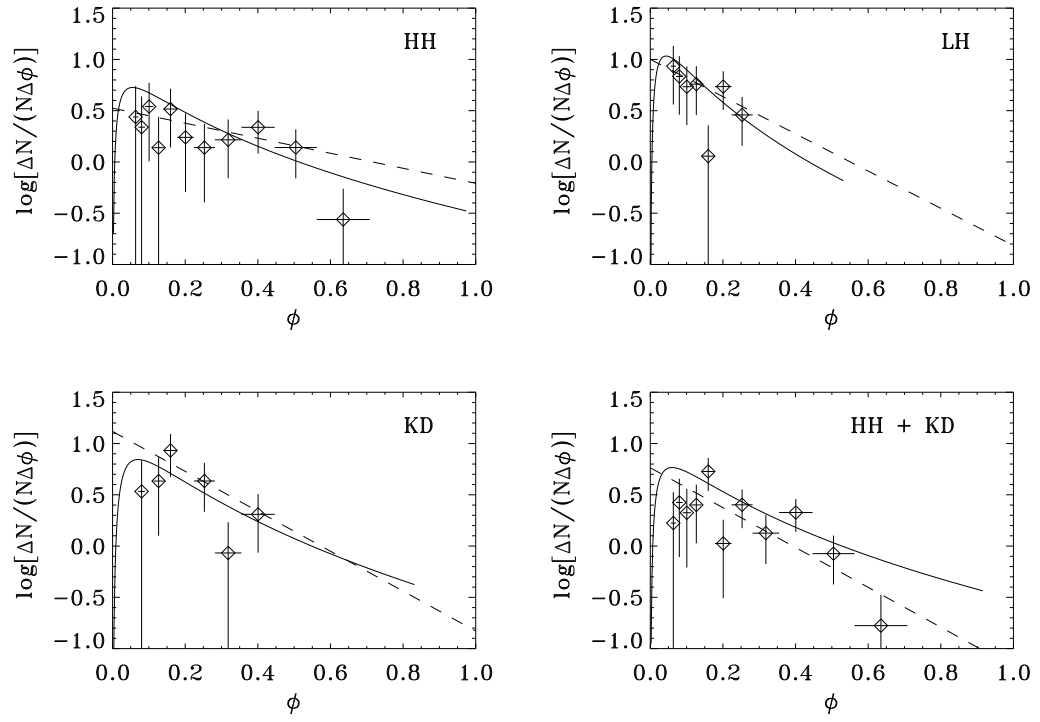


Figure 7: As in Fig. 3, but concerning calcium instead of oxygen.

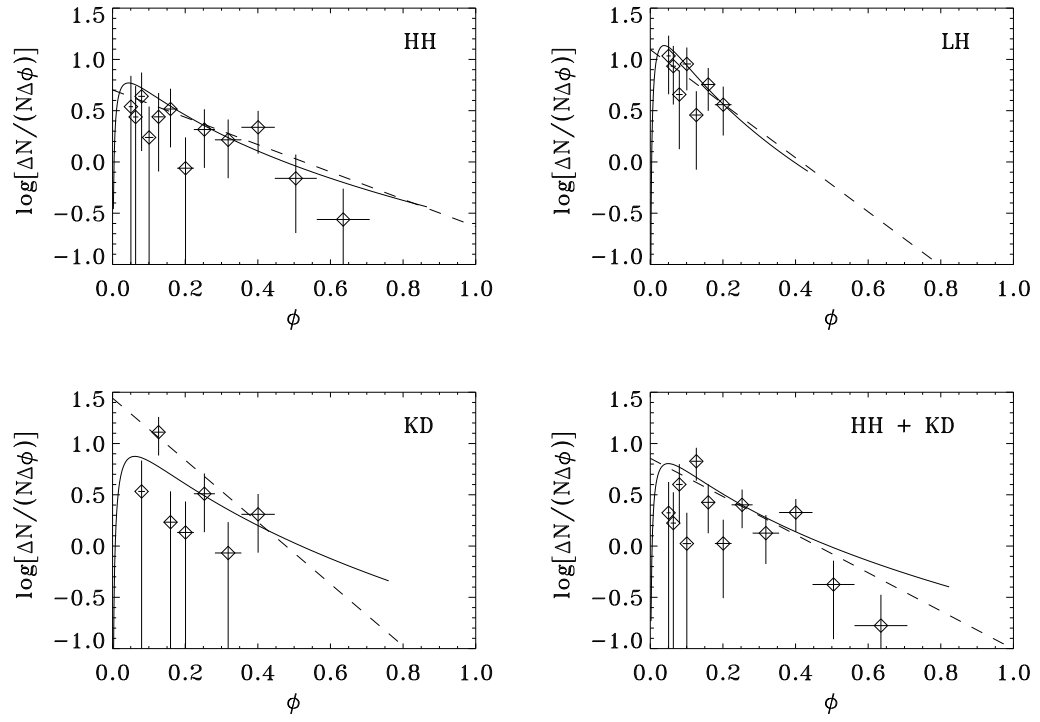


Figure 8: As in Fig. 3, but concerning titanium instead of oxygen.

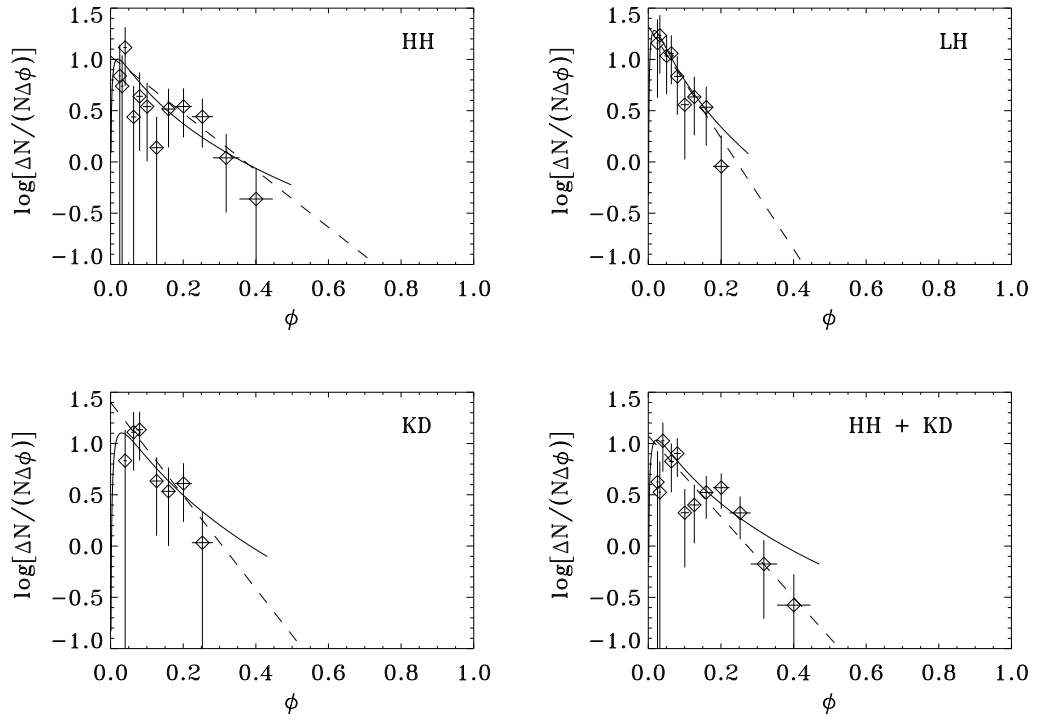


Figure 9: As in Fig. 3, but concerning chromium instead of oxygen.

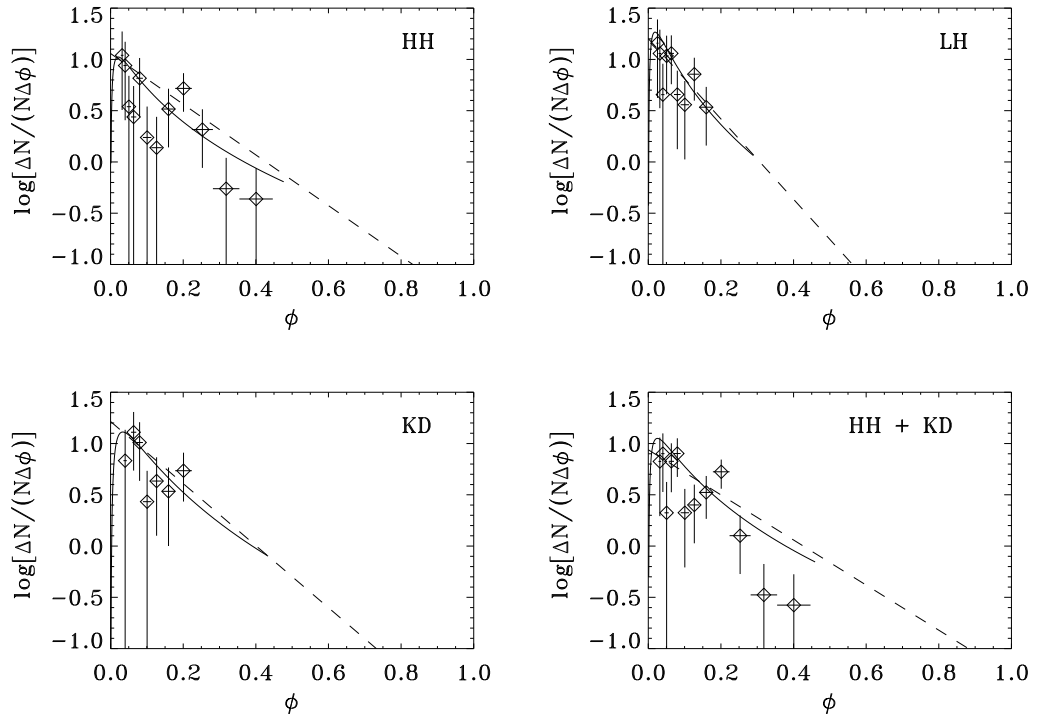


Figure 10: As in Fig. 3, but concerning iron instead of oxygen.

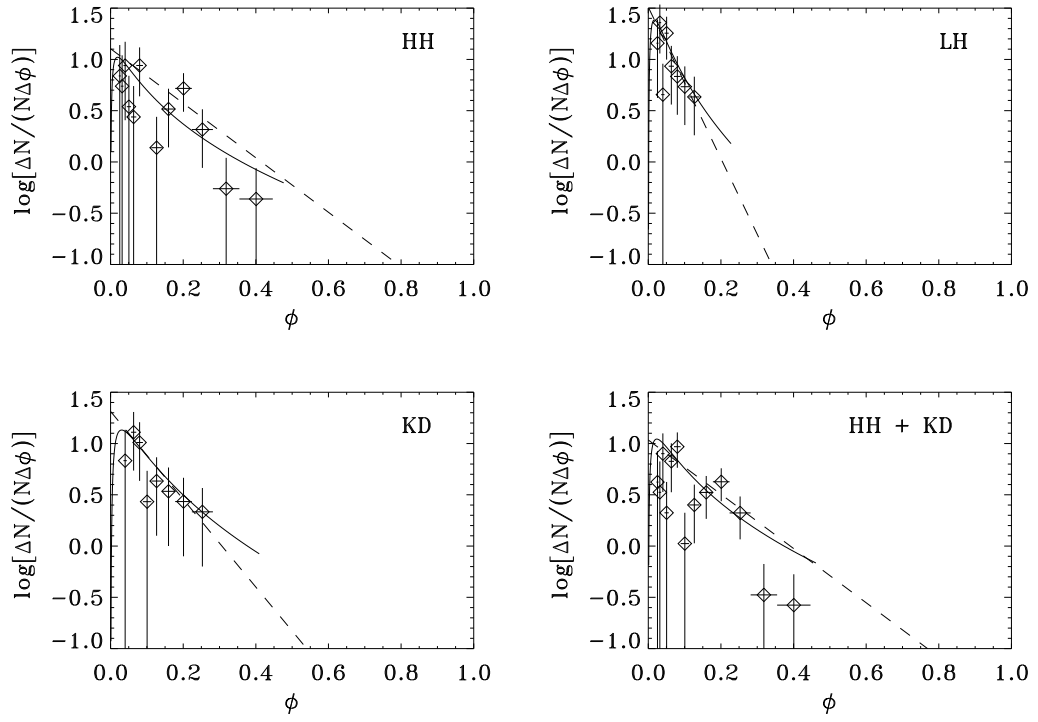


Figure 11: As in Fig. 3, but concerning nikel instead of oxygen.

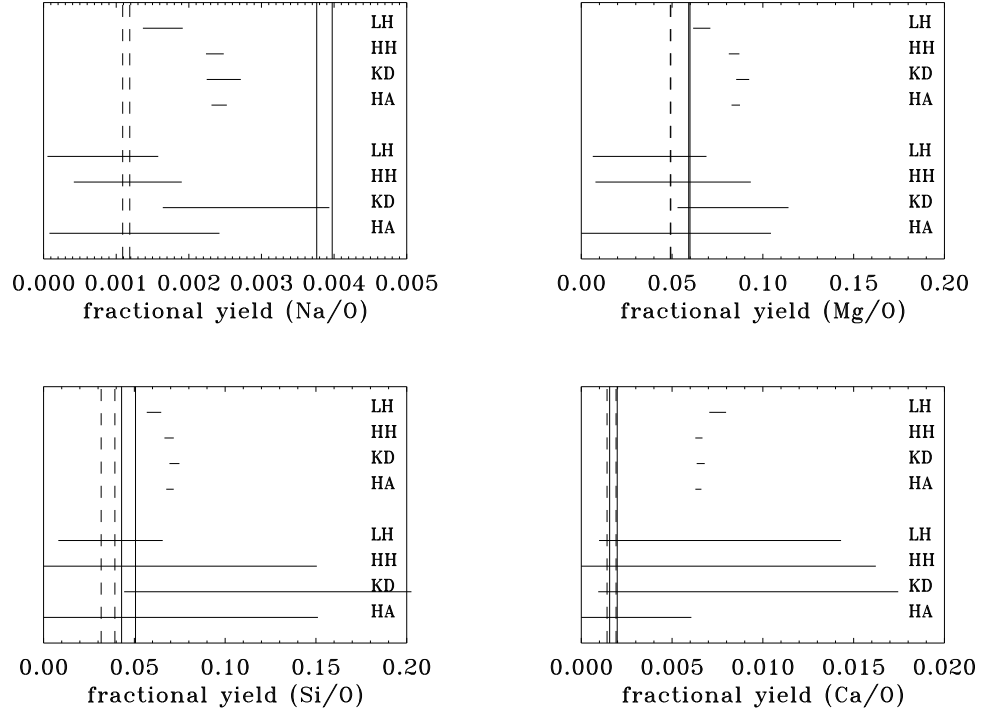


Figure 12: Comparison between the fractional yield, \hat{p}_Q/\hat{p}_O , $Q = \text{Na, Mg, Si, Ca}$, inferred from Eqs. (14) and (18), for different subsamples as indicated (top and bottom bars, respectively) and theoretical counterparts deduced from stellar nucleosynthesis (vertical bands) for solar, $Z = Z_{\odot}$ (full), and subsolar, $Z = Z_{\odot}/10$ (dashed) metallicity, under the assumption of a power-law stellar initial mass function. The bar semiamplitude equals $2\sigma_{\hat{p}_Q/\hat{p}_O}$. The band width relates to a fiducial range of power-law exponent, $-3 \leq -p \leq -2$. See text for further details.

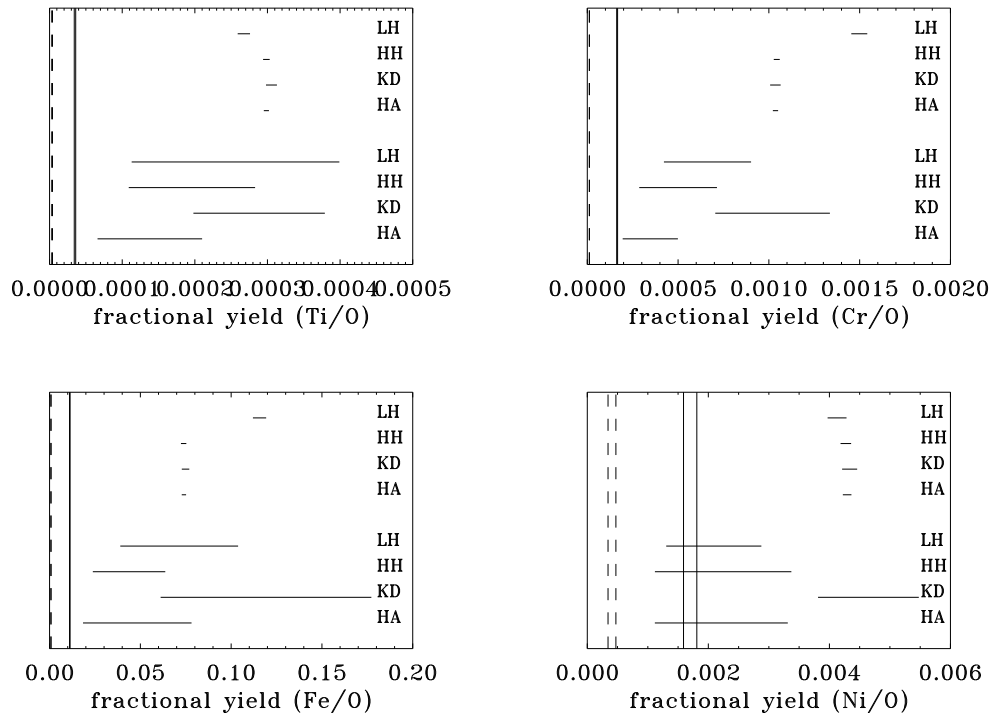


Figure 13: As in Fig. 12, but for $Q = \text{Ti, Cr, Fe, Ni}$.

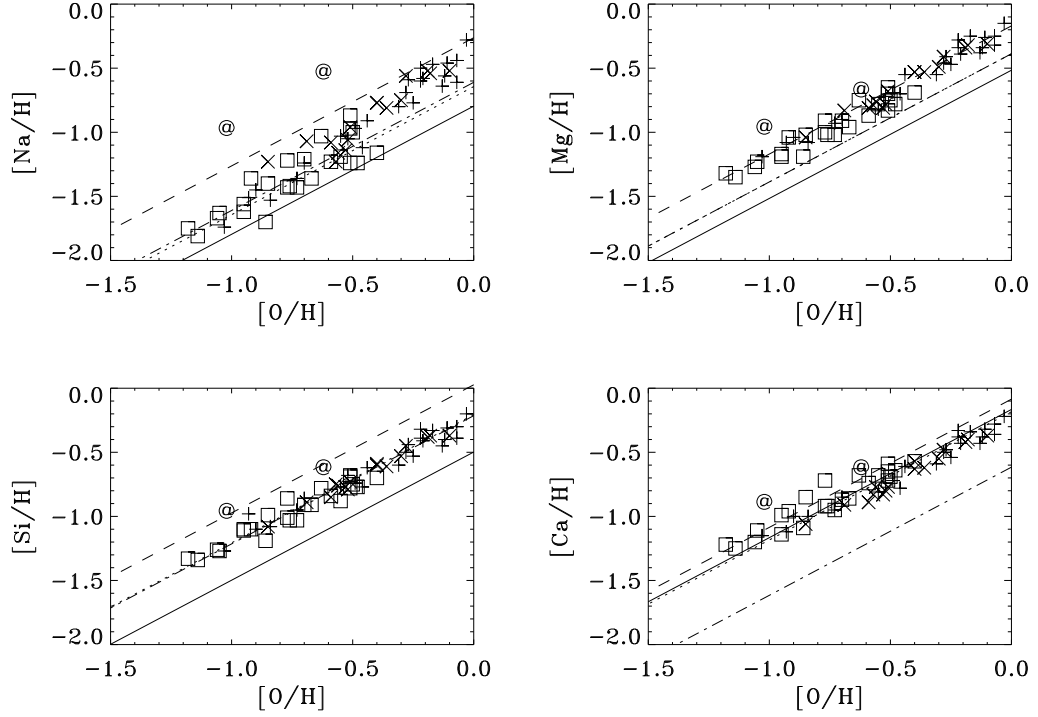


Figure 14: The theoretical $[Q/H]$ - $[O/H]$ relation, $Q = \text{Na, Mg, Si, Ca}$, inferred from simple MCBR models, via Eq. (19), for subsamples, LH (low- α halo stars, full lines), HH (high- α halo stars, dotted lines), KD (low-metallicity thick disk stars, dashed lines), HA (high- α halo + low-metallicity thick disk stars, dot-dashed lines). Subsample stars are also plotted with same symbols as in Fig. 1. See text for further details.

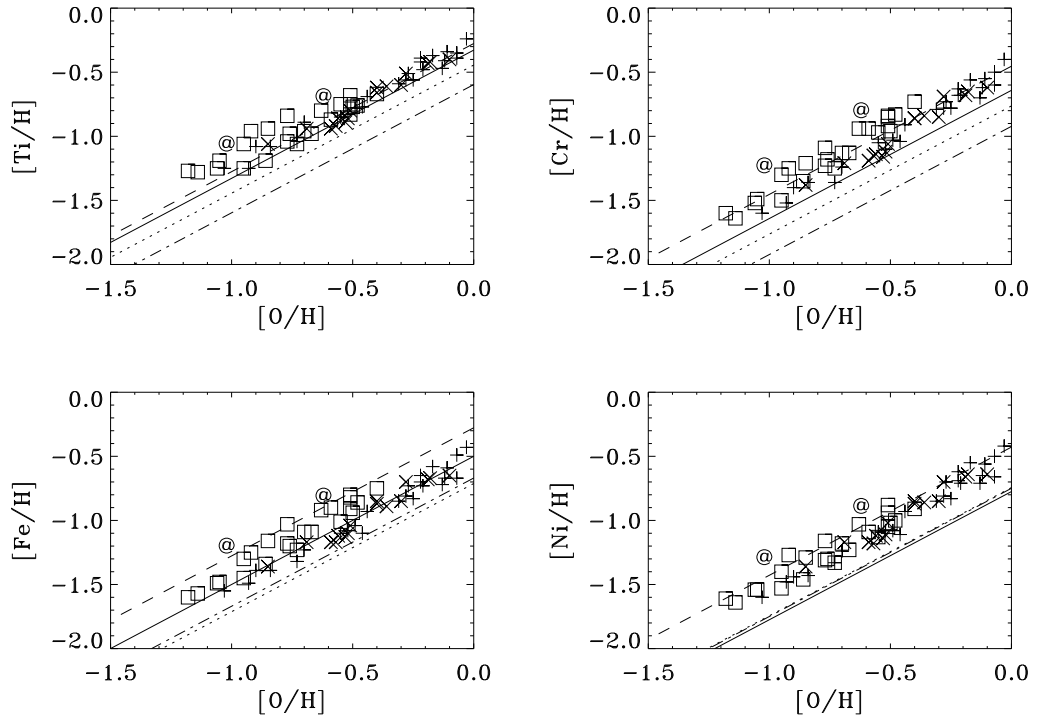


Figure 15: As in Fig. 14, but for $Q = Ti, Cr, Fe, Ni$.